ARCHIVES OF MECHANICS
Arch. Mech. **73** (3), 267–300, 2021, DOI: 10.24423/aom.3732

# Absolute instability of double annular jets: local stability analysis

A. BOGUSLAWSKI, K. WAWRZAK

*Department of Thermal Machinery, Częstochowa University of Technology, Faculty of Mechanical Engineering and Computer Science, Armii Krajowej 21, 42-201 Częstochowa, Poland, e-mail: abogus@imc.pcz.pl*

The paper presents the local linear stability analysis of the double annular jets. The calculations show that the first absolutely unstable helical mode can be generated in the non-swirling annular jets by the back-flow in the central recirculation zone or sufficiently strong back-flow in the external recirculation zone. The influence of the back-flow magnitude on the frequency, growth rate and eigenfunctions of the first helical mode is discussed. The calculations are completed with an analysis of the influence of the swirl intensity in the internal and external jets on the characteristics of the first absolutely unstable helical mode.

**Key words:** stability analysis, annular jets.



## 1. Introduction

Annular nozzles are used in many technical applications as in gas turbines and aeroengines to deliver fuel and oxidiser in a combustion chamber. An annular jet issuing from such a nozzle is seemingly a simple flow type, although the dynamics of large scale structures appearing in this flow has not been fully understood till now despite an enormous number of theoretical, experimental and numerical studies in this field. Large scale structures in the transitional region of the annular jet could enhance or deteriorate mixing intensity in combustors, hence improved understanding of the flow dynamics could be helpful in the development of new and more efficient combustion technologies. As observed experimentally in various combustors the flow is dominated by spiral large scale structures. These structures stem from a phenomenon called the vortex breakdown (VB) [1]. Although the VB has already been studied for more than six decades, in all possible ways: theoretically, experimentally and numerically, its origin has not been fully recognised so far. The VB is a highly time-dependent phenomenon and the spiral-shaped structures start to precess about the jet axis thus forming the so-called precessing vortex core (PVC) [2]. As pointed out in [3] the theories proposed for the VB could be categorised into the following concepts:

1. The phenomenon is associated with the concept of critical state or, more generally, with wave phenomena [4–6].
2. The phenomenon is analogous to boundary layer separation or flow stagnation [7, 8].
3. The phenomenon is a consequence of the hydrodynamic instability [9–12].

There are many more recent advanced approaches to the VB especially in the case of swirling jets [13] and swirling annular jets [14, 15] indicating that the Kelvin-Helmholtz instability could be the major source of spiral structures in these flow types. The VB has been observed in many flow types like circular jets and annular jets with a swirl and it seems that the origin of this phenomenon has not been fully understood so far. As stressed by Vaniershot *et al.* [16] due to the occurrence of several types of breakdown and the often contradictory results because of high sensitivity to boundary conditions, there is still no consensus about the origin of the VB.

Recently one can find many opinions in the literature [17–19] based on experimental results and stability calculations indicating that the VB is actually the manifestation of the self-excited global hydrodynamic instability triggered by the absolutely unstable helical modes.

Michalke [20] using spatio-temporal stability theory and Briggs/Bers criteria [21–23] showed a presence of the first azimuthal absolutely unstable mode in both non-swirling and swirling annular jets. Parametric studies of annular jet stability were performed by Boguslawski and Wawrzak [24]. They showed that the steepness of the inner shear layer promoted absolute instability and had a weak influence on the absolute mode frequency. On the contrary, the steepness of the outer shear layer did not influence the absolute growth rate while it led to a certain decrease in the oscillations frequency. The calculations performed confirmed also conclusions derived by Michalke [20] that a stronger back-flow promoted the absolute growth rate and that a limited amount of swirl promoted the first helical absolute mode.

Qualitative results stemming from the parametric studies of Boguslawski and Wawrzak [24] were utilised by Wawrzak *et al.* [25] in their Large Eddy Simulations (LES) studies of a non-swirling annular jet. They showed that helical structures could be triggered by varying the steepness of the inner shear layer confirming the results of the stability theory.

A more common configuration used in gas turbines and aeroengine combustors consists of two coaxial annular jets. A mean velocity field of such a flow type was studied experimentally [26, 27] and numerically [28]. However, the dynamics of large scale structures in the double annular jets seems to be little known. Such a fact is surprising taking into account common industrial applications of this flow type. Preliminary stability calculations of the double annular non-swirling

jets were performed by BIJAK and BOGUSLAWSKI [29], however, limited to a narrow range of the governing parameters. It is known from the measurements that the flow field is characterised by a central recirculation zone (CRZ) behind the central bluff body and a concentric external recirculation zone (ERZ) formed by the external annular jet. As it is known from previous studies, based on the stability theory [20, 24] and LES predictions [25], the back-flow in the CRZ is favourable for triggering the absolutely unstable helical modes. Hence, it is interesting whether the jet stability can be also controlled by a back-flow in the ERZ, in double annular jets. The present study is aimed at a stability analysis of the double annular jets to understand what is the impact of the external annular jet on the first azimuthal absolutely unstable mode and to establish favourable conditions for such instability in non-swirling and swirling flows.

## 2. Base flow

A schematic view of the double annular jet is shown in Fig. 1. The internal annular jet is characterised by the outer and inner diameters denoted by $D_o^{int}$ and $D_i^{int}$, respectively. Behind the bluff body, the CRZ is formed that is surrounded by the inner shear layer. The outer one is formed between the jet and the ERZ formed behind the annular bluff body between internal and external nozzles. The external annular jet is characterised by the outer and inner diameters denoted by $D_o^{ext}$ and $D_i^{ext}$, respectively. Sample axial and tangential velocity profiles in the cross-section denoted by the dashed line are also shown. All the velocities are normalised by the maximum axial velocity in the internal jet and all the lengths by the radius where this maximum appears. In the case of the local stability analysis, it is assumed that the flow is parallel and the velocity field extends infinitely along the jet axis. Thus the base flow of the annular jet is modelled by an axial velocity $U(r)$ and a swirl with the tangential velocity component $W(r)$. In a parallel flow approximation, the radial velocity component $V(r)$ is neglected. The axial velocity component $U(r)$ represents a double annular jet with a possible reversed flow on the jet axis with $U(r=0) = U_0 < 0$ and a back-flow in the ERZ with $U_{01} < 0$.

A flexible method to describe axial and tangential velocity profiles in a vicinity of the annular nozzle exit was proposed by BOGUSLAWSKI and WAWRZAK [24]. To approximate the axial velocity profile the hyperbolic tangent function was applied. This function was used to describe the shear layer velocity profile in the case of counter-current jets by JENDOUBI and STRYKOWSKI [30] and in the case of a hot jet by BOGUSLAWSKI *et al.* [31]. It was shown in the latter work that the hyperbolic tangent function reproduced well velocity profiles resulting from LES. In this section, the analysis is extended to the problem of the double annular jet with a swirl. The laminar base flow characterising such a flow should be flexible

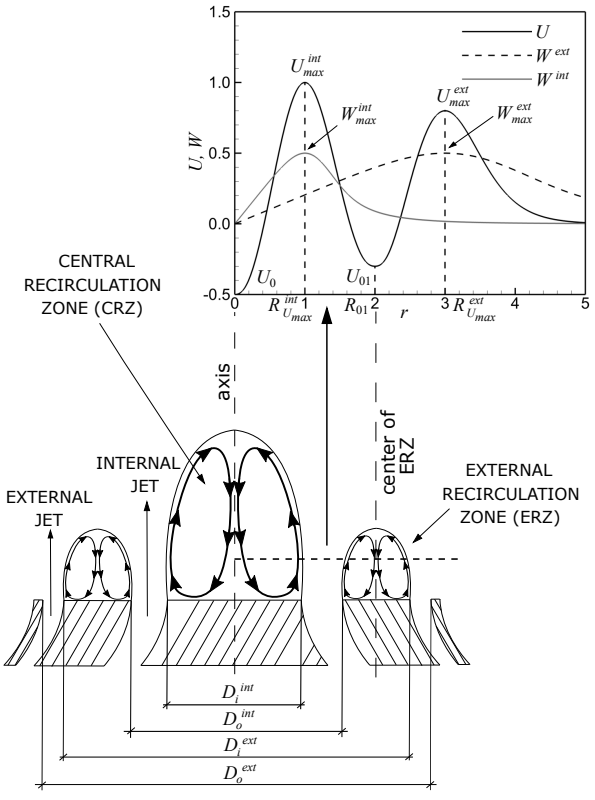


FIG. 1. Schematic view of the double annular jet indicating central and external recirculation zones.

allowing independent control of the velocity profiles of the internal and external jets. The only constraint is zero radial velocity gradient at the jet axis and in the middle of the ERZ. Other parameters like velocity gradients in shear layers, back-flow velocities in recirculation zones, maximum velocities and their location in both jets should be defined independently. The same refers to the tangential velocity profiles. In this case, the only constraint was the continuous first radial derivative. As it was shown in [24] for a single annular jet the axial velocity profile built from hyperbolic tangent functions satisfies all the requirements. Hence, a similar approach to approximate the laminar base flow for the double annular jet with a swirl is discussed in the paper. The flow is modelled for internal and external jets by independent functions. The internal annular jet extends from the axis to the radius $R_{01}$ in the centre of the ERZ and the external one from $R_{01}$ to infinity. Hence, the axial velocity profile is defined as

$$U(r) = \begin{cases} U^{int}(r) & \text{for } 0 < r \leq R_{01}, \\ U^{ext}(r) & \text{for } R_{01} < r < \infty. \end{cases} \tag{2.1}$$

Velocity profiles for the internal and external jets are described by the following functions:

$$
\begin{aligned}
(2.2)\qquad U^{int}(r) &= U^{int}_{in}\tanh[b^{int}_{in}(r-R^{int}_{in})] - U^{int}_{out}\tanh[b^{int}_{out}(r-R^{int}_{out})] \\
&+ \frac{b^{int}_{in}U^{int}_{in}}{\cosh^2(-b^{int}_{in}R^{int}_{in})}\frac{[1-\tanh(b^{0,int}_{in}r)]}{b^{0,int}_{in}} - \frac{b^{int}_{out}U^{int}_{out}}{\cosh^2(-b^{int}_{out}R^{int}_{out})}\frac{[1-\tanh(b^{0,int}_{out}r)]}{b^{0,int}_{out}} \\
&- \frac{b^{int}_{in}U^{int}_{in}}{\cosh^2[b^{int}_{in}(R_{01}-R^{int}_{in})]}\frac{\{1-\tanh[b^{0,int}_{in}(-r+R_{01})]\}}{b^{0,int}_{in}} \\
&+ \frac{b^{int}_{out}U^{int}_{out}}{\cosh^2[b^{int}_{out}(R_{01}-R^{int}_{out})]}\frac{\{1-\tanh[b^{0,int}_{out}(-r+R_{01})]\}}{b^{0,int}_{out}} \\
&- U^{int}_{in} + U^{int}_{out} + U^{int}_{\infty}
\end{aligned}
$$

and

$$
\begin{aligned}
(2.3)\qquad U^{ext}(r) &= U^{ext}_{in}\tanh[b^{ext}_{in}(r-R^{ext}_{in})] - U^{ext}_{out}\tanh[b^{ext}_{out}(r-R^{ext}_{out})] \\
&+ \frac{b^{ext}_{in}U^{ext}_{in}}{\cosh^2[b^{ext}_{in}(R_{01}-R^{ext}_{in})]}\frac{\{1-\tanh[b^{0,ext}_{in}(r-R_{01})]\}}{b^{0,ext}_{in}} \\
&- \frac{b^{ext}_{out}U^{ext}_{out}}{\cosh^2[b^{ext}_{out}(R_{01}-R^{ext}_{out})]}\frac{\{1-\tanh[b^{0,ext}_{out}(r-R_{01})]\}}{b^{0,ext}_{out}} \\
&- U^{ext}_{in} + U^{ext}_{out},
\end{aligned}
$$

the subscripts "*in*" and "*out*" in Eqs. (2.2) and (2.3) refer to inner and outer shear layers, while superscripts "*int*" and "*ext*" stand for the internal and external jets. The parameters $b^{int}_{in}$, $b^{int}_{out}$ and $b^{ext}_{in}$, $b^{ext}_{out}$ allow the control of the velocity gradients in inner and outer shear layers of both internal and external jets. The details of procedures to establish the parameters of the axial velocity profiles are described in Appendix A.

To complete the description of the laminar base flow a tangential velocity profile for a double annular jet must be defined. It is proposed as a superposition of two Lamb-Oseen generalised vortices, used already in [24], as:

$$
(2.4)\qquad W(r) = W^{int}(r) + W^{ext}(r),
$$

where

$$
(2.5)\qquad W^{int}(r) = \frac{A^{int}(R^{int}_{W_{max}})^{N^{int}_W-1}}{r^{N^{int}_W-1}}\left\{\frac{1-\exp(-b^{int}r^{N^{int}_W})}{1-\exp[-b^{int}(R^{int}_{W_{max}})^{N^{int}_W}]}\right\},
$$

$$
(2.6)\qquad W^{ext}(r) = \frac{A^{ext}(R^{ext}_{W_{max}})^{N^{ext}_W-1}}{r^{N^{ext}_W-1}}\left\{\frac{1-\exp(-b^{ext}r^{N^{ext}_W})}{1-\exp[-b^{ext}(R^{ext}_{W_{max}})^{N^{ext}_W}]}\right\},
$$

where $A^{int} = W^{int}_{max}/U^{int}_{max}$ and $A^{ext} = W^{ext}_{max}/U^{int}_{max}$ are swirl numbers in the internal and external jets, respectively. The symbols $R^{int}_{W_{max}}$ and $R^{ext}_{W_{max}}$ denote the radii for which azimuthal velocity attains its maximum in the internal and external jets, respectively. The exponents $N^{int}_W$ and $N^{ext}_W$ control the decay rate of the velocity at the vortex peripheries, for internal and external vortices, while in the vortex core the velocity is still close to the solid body rotation.

The parameters $b^{int}$ and $b^{ext}$ are found from the conditions that the functions (2.5) and (2.6) have the maximum at the radii $r = R^{int}_{W_{max}}$ and $r = R^{ext}_{W_{max}}$, respectively.

## 3. Stability equations and solution method

The small disturbance of flow parameters is assumed as a wave travelling along axial $x$ and azimuthal $\varphi$ directions with the amplitude varying along with the radial direction $r$ in the following form:

$$(u', v', w', p') = [\hat{u}(r), \hat{v}(r), \hat{w}(r), \hat{p}(r)] \exp[i(\alpha x + m\varphi - \omega t)]. \tag{3.1}$$

Here $u', v', w'$ and $p'$ are axial, radial, azimuthal velocity and pressure disturbances, respectively, $\alpha = \alpha_r + i\alpha_i$ is the complex wavenumber, $\omega = \omega_r + i\omega_i$ is the complex frequency and $m$ is the azimuthal real wavenumber. Such disturbances are introduced into the continuity equation and Euler equations in cylindrical coordinates and linearised around the given base flow. As shown by MICHALKE [20], after eliminating the $\hat{u}$ and $\hat{w}$ velocities, the stability equations can be written as

$$r\sigma \frac{d\hat{p}}{dr} = i[2WZ - r\sigma^2]\hat{v} - \frac{2mW}{r}\hat{p}, \tag{3.2}$$

$$\frac{\sigma}{r}\frac{d(r\hat{v})}{dr} = i\left[\alpha^2 + \frac{m^2}{r^2}\right]\hat{p} + \left[\alpha\frac{dU}{dr} + m\frac{Z}{r}\right]\hat{v}, \tag{3.3}$$

where

$$\sigma(r) = \alpha U - \omega + \frac{W}{r}m, \tag{3.4}$$

$$Z(r) = \frac{dW}{dr} + \frac{W}{r}. \tag{3.5}$$

To solve the system of the stability equations (3.2) and (3.3) the boundary conditions must be formulated on the jet axis $r = 0$ and for $r \to \infty$ using features of the axial and azimuthal velocity profiles of the base flow. The boundary conditions require that $\hat{v}(r)$ and $\hat{p}(r)$ are bounded on the jet axis and both quantities

vanish at the jet periphery. The asymptotic behaviour for $r \to \infty$ can be obtained if one takes into account that

$$\lim_{r\to\infty} U, \quad \frac{dU}{dr}, \quad Z = 0, \quad \lim_{r\to\infty} \frac{W}{r} = \frac{A_\infty^{int}}{r^{N_W^{int}}} + \frac{A_\infty^{ext}}{r^{N_W^{ext}}}, \tag{3.6}$$

where

$$A_\infty^{int} = \frac{A^{int}(R_{W_{max}}^{int})^{N_W^{int}-1}}{1-\exp[-b^{int}(R_{W_{max}}^{int})^{N_W^{int}-1}]}, \quad A_\infty^{ext}\frac{A^{ext}(R_{W_{max}}^{ext})^{N_W^{ext}-1}}{1-\exp[-b^{ext}(R_{W_{max}}^{ext})^{N_W^{ext}-1}]}.$$

Introducing the notation:

$$\sigma_\infty = \lim_{r\to\infty}\sigma(r) = m\left(\frac{A_\infty^{int}}{r^{N_W^{int}}} + \frac{A_\infty^{ext}}{r^{N_W^{ext}}}\right) - \omega, \tag{3.7}$$

the stability equations (3.2) and (3.3) for $r \to \infty$ take the following forms:

$$r\sigma_\infty\frac{d\hat{p}}{dr} = -ir\sigma_\infty^2\hat{v} - 2m\left(\frac{A_\infty^{int}}{r^{N_W^{int}}} + \frac{A_\infty^{ext}}{r^{N_W^{ext}}}\right)\hat{p}, \tag{3.8}$$

$$\frac{\sigma_\infty}{r}\frac{d(r\hat{v})}{dr} = i\left[\alpha^2 + \left(\frac{m}{r}\right)^2\right]\hat{p}. \tag{3.9}$$

Introducing the notation $\Phi = r\hat{v}$ Eq. (3.9) reads as

$$\frac{d}{dr}\left[\frac{r}{m^2+(\alpha r)^2}\frac{d\Phi}{dr}\right] - \frac{\Phi}{r} = 0 \tag{3.10}$$

with the decaying solution

$$\Phi = rK_m'(\alpha r), \tag{3.11}$$

where $K_m$ is the modified Bessel function of the second kind and order $m$. Hence, $\hat{v}$ velocity at the limit $r \to \infty$ is

$$\hat{v}(r) = K_m'(\alpha r). \tag{3.12}$$

As shown by MICHALKE [20], neglecting the second term on r.h.s of Eq. (3.8), for $r \to \infty$, and integrating leads to the asymptotic limit for a pressure perturbation at the jet periphery

$$\hat{p}(r) = -\frac{i}{\alpha}\sigma_\infty K_m(\alpha r) = -\frac{i}{\alpha}\left[m\left(\frac{A_\infty^{int}}{r^{N_W^{int}}} + \frac{A_\infty^{ext}}{r^{N_W^{int}}}\right) - \omega\right]K_m(\alpha r). \tag{3.13}$$

The boundary conditions on the jet axis, despite a different base flow used in the current analysis, are the same as shown by MICHALKE [20]. Pressure and velocity perturbations at the jet axis are expressed as

$$\hat{p}(r) = I_m(\beta r), \tag{3.14}$$

$$\hat{v}(r) = \frac{i\alpha}{\sigma_0\sqrt{1-\mu^2}}\left[I'_m(\beta r) + \frac{m\mu}{\beta r} I_m(\beta r)\right], \tag{3.15}$$

where $I_m$ is the modified Bessel function of the first kind and

$$\Omega = A_\infty^{int} b^{int} + A_\infty^{ext} b^{ext}, \quad \sigma_0 = \alpha U_0 - \omega, \quad \mu = \frac{2\Omega}{\sigma_0}, \quad \beta^2 = \alpha^2(1-\mu^2). \tag{3.16}$$

The eigenvalue problem now is solved numerically by integrating stability equations (3.2) and (3.3) by means of the Runge–Kutta–Fehlberg procedure [32] of the 4th order starting with $r = 10^{-6}$ and boundary conditions (3.14) and (3.15) up till $r = 1$ yielding $\hat{p}_L(1)$ and $\hat{v}_L(1)$, and from a radius $r_\infty$, large enough to apply the asymptotic solutions (3.12) and (3.13), back to $r = 1$ yielding $\hat{p}_R(1)$ and $\hat{v}_R(1)$. The eigenvalue condition then follows from the matching of these solutions at $r = 1$, requiring:

$$G(\omega, \alpha) = \frac{\hat{p}_L}{\hat{v}_L} - \frac{\hat{p}_R}{\hat{v}_R} = 0. \tag{3.17}$$

This condition leads, for a given $\omega$, to a relation $\alpha(\omega)$, or, for a given $\alpha$ to $\omega(\alpha)$. The eigenvalue problems can be solved by Newton's method [33] as

$$\omega^{(n+1)} = \omega^{(n)} - \frac{G(\omega^{(n)}, \alpha)}{\partial G/\partial\omega|_{\omega^{(n)}}}, \tag{3.18}$$

$$\alpha^{(n+1)} = \alpha^{(n)} - \frac{G(\omega, \alpha^{(n)})}{\partial G/\partial\alpha|_{\alpha^{(n)}}}, \tag{3.19}$$

where

$$\frac{\partial G}{\partial\omega} = \frac{1}{\hat{v}_L}\left(\frac{\partial\hat{p}}{\partial\omega}\right)_L - \frac{1}{\hat{v}_R}\left(\frac{\partial\hat{p}}{\partial\omega}\right)_R - \frac{\hat{p}_L}{\hat{v}_L^2}\left(\frac{\partial\hat{v}}{\partial\omega}\right)_L + \frac{\hat{p}_R}{\hat{v}_R^2}\left(\frac{\partial\hat{v}}{\partial\omega}\right)_R, \tag{3.20}$$

$$\frac{\partial G}{\partial\alpha} = \frac{1}{\hat{v}_L}\left(\frac{\partial\hat{p}}{\partial\alpha}\right)_L - \frac{1}{\hat{v}_R}\left(\frac{\partial\hat{p}}{\partial\alpha}\right)_R - \frac{\hat{p}_L}{\hat{v}_L^2}\left(\frac{\partial\hat{v}}{\partial\alpha}\right)_L + \frac{\hat{p}_R}{\hat{v}_R^2}\left(\frac{\partial\hat{v}}{\partial\alpha}\right)_R. \tag{3.21}$$

In order to use Newton's method to solve an eigenvalue problem one needs information on the derivatives of pressure and velocity perturbations with respect to the complex wavenumber $\alpha$ or the complex frequency $\omega$, respectively. This information can be obtained solving the differential equations obtained from the stability equations (3.2), (3.3) and the boundary conditions (3.12), (3.13), (3.14) and (3.15) differentiated with respect to the wavenumber $\alpha$ or the frequency $\omega$, respectively.

## 4. Results

### 4.1. Non-swirling jets

Velocity profiles analysed within the present work for double annular jets were based on the velocity profiles of a single annular jet analysed in [24]. The stability calculations were performed for three back-flow velocities in the CRZ, namely $U_0 = 0, -0.3, -0.5$. In the case $U_0 = 0$ the jet without a swirl or an external annular jet is not in the absolutely unstable regime while two other cases are absolutely unstable [20]. The parameters of axial velocity radial gradients in the inner and outer shear layers of the internal jet were kept constant $b_{in}^{int} = b_{out}^{int} = 1.5$. The same values were used for the external jet $b_{in}^{ext} = b_{out}^{ext} = 1.5$. The parameters $b_{in}^{0,int} = b_{out}^{0,int} = b_{in}^{0,ext} = b_{out}^{0,ext} = 4.0$ were kept also fixed in all the test cases analysed. The centre of the ERZ was chosen as $R_{01} = 2$ and the radius of the maximum velocity in the external jet $R_{U_{max}}^{ext} = 3.0$. As the main goal of the present work was to analyse the influence of the external annular jet on the flow stability only the parameters changing the ERZ were changed. The parameters $R_{in}^{int} = 0.75$ and $R_{out}^{ext} = 3.25$ were applied for the test cases with the back-flow velocities in the CRZ $U_0 = 0$ and $U_0 = -0.3$ while in the case of $U_0 = -0.5$ the parameter was slightly lower $R_{in}^{int} = 0.70$ as for this back-flow for $R_{in}^{int} = 0.75$ the convergent solution for $U_{in}^{int}$ was not found. All other parameters controlling the ERZ, imposed and calculated, as shown before, will be presented for each test case. Following the work of MICHALKE [20] the stability analysis of the first azimuthal mode ($m = 1$) was performed. This mode seems to be of primary importance in practical applications since in gas turbines and aeroengines this type of instability could trigger helical structures responsible for the enhancement of mixing of fuel and oxidiser streams. The second helical mode ($m = 2$) was studied by BOGUSLAWSKI and WAWRZAK [24] and they showed that this mode, which could trigger double helical structures, was present only for strongly swirling flows.

Figure 2 shows iso-contours of the imaginary part of the complex frequency $\omega_{0,i}$ around a saddle point $d\omega/d\alpha = 0$ in complex wavenumbers plane where the pinching condition is satisfied. Having known the $\omega$-maps in $\alpha$-planes around the saddle point, the precise pairs $\omega_0$ and $\alpha_0$, for which $d\omega/d\alpha = 0$, were found using an iterative procedure presented by MONKEWITZ and SOHN [34]. The results shown in Fig. 2 correspond to the test case $BF_0^{int}BF_{02}^{ext}$ ($BF^{int}$ and $BF^{ext}$ stand for the back-flow velocity magnitudes in the CRZ and ERZ, respectively), defined in Table B.1, for which the first helical mode is absolutely unstable. Numerical values of the complex wavenumbers $\alpha_0$ and frequencies $\omega_0$ for all the test cases considered in the paper are shown in Appendix C.

The velocity profiles for the test cases with $U_0 = 0$ are shown in Fig. 3a, with the list of parameters of the axial velocity profiles gathered in Table B.1.

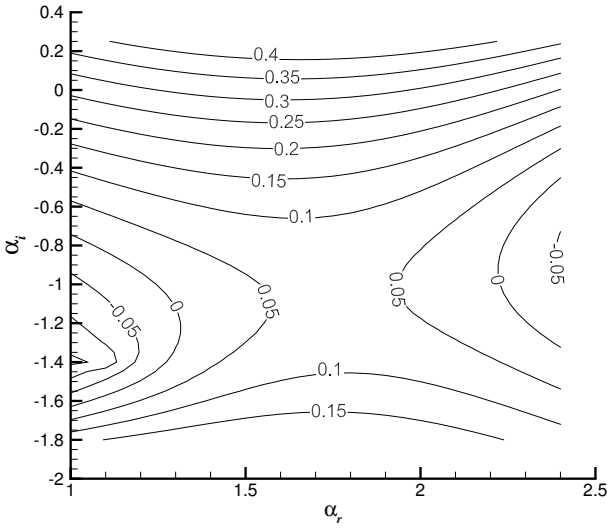


FIG. 2. Iso-contours of the imaginary part of the complex frequency $\omega_i$ around a saddle point $d\omega/d\alpha = 0$ in complex wave numbers plane, test case $BF_0^{int}BF_{02}^{ext}$.

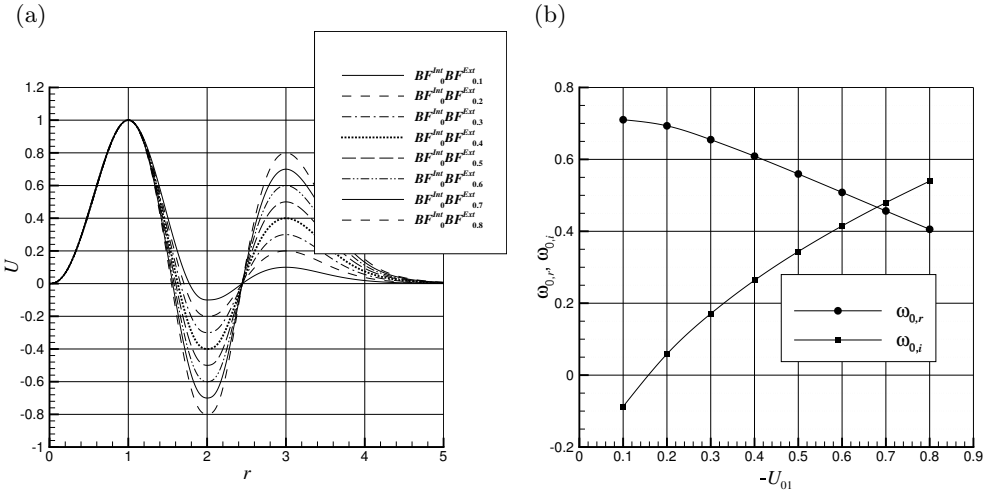


FIG. 3. Influence of the back-flow velocity in the ERZ, $U_0 = 0$: (a) axial velocity profiles, (b) complex frequency of the first absolute helical mode.

Figure 3b shows the complex frequency $\omega_0$ as a function of the back-flow velocity in the ERZ. It is seen that the absolute mode temporal growth rate $\omega_{0,i}$ for the smallest back-flow velocity in the ERZ $U_{01} = -0.1$ is negative. A stronger back-flow in the ERZ promotes the first helical absolute mode and absolute instability is triggered for the back-flow velocity $U_{01} \approx -0.158$. Further increase of the external back-flow magnitude is favourable for the absolute mode growth

rate. The increasing growth rate is associated with a substantial decrease of the absolute mode frequency $\omega_{0,r}$.

Figure 4 shows the eigenfunctions for pressure and velocity perturbations generated by the first helical mode. The eigenfunctions are shown in the form of their magnitude related to the maximum value. It can be seen that the pressure perturbation is concentrated around the outer shear layer of the internal jet. The local maximum in the inner shear layer is decreasing with respect to the peak in the outer shear layer along with the back-flow strength in the ERZ. The maximum of the velocity perturbations for a weak back-flow in the ERZ is located at the jet axis and is gradually moving to the centre of the ERZ along with an increased back-flow velocity magnitude.

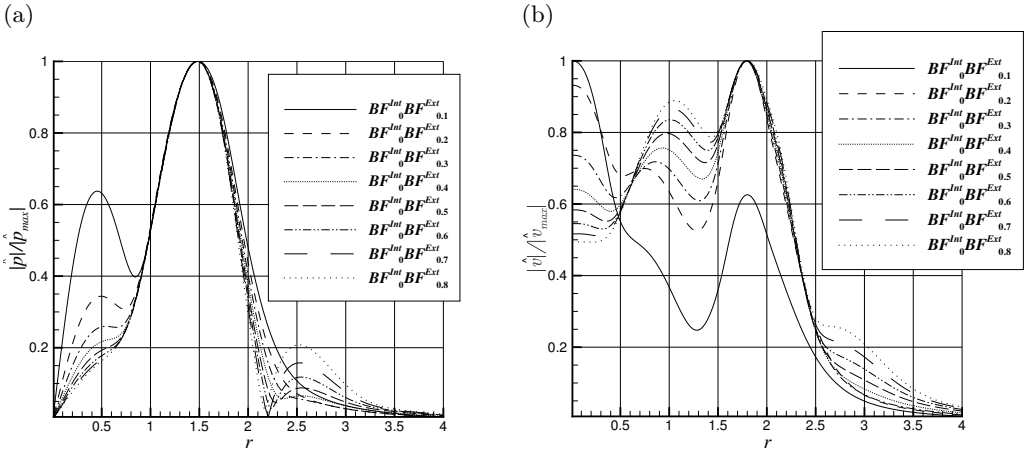


FIG. 4. Influence of the back-flow velocity in the ERZ on eigenfunctions of the first helical absolute mode, $U_0 = 0$: (a) pressure perturbation, (b) velocity perturbation.

In all the cases discussed above, it was assumed that the maximum velocity magnitude in the external jet is equal to the magnitude of the back-flow in the external recirculations zone. In real jets, a relation between the maximum velocity and strength of the back-flow depends on a few factors: the Reynolds number, the shape of the nozzle, width of the annular bluff body between jets. Hence, it is an important question of how the flow instability depends on the maximum velocity for a given back-flow in the ERZ. Velocity profiles for such test cases are shown in Fig. 5a. The parameters of axial velocity profile for the internal jet are exactly the same as for the test case $BF_0^{int}BF_{05}^{ext}$ and the parameters for the external jet are shown in Table B.2. The complex frequency of the first helical absolutely unstable mode for a varying maximum velocity of the external jet is shown in Fig. 5b. It is seen that for a given back-flow in the ERZ, $U_{01} = -0.5$ in this case, increasing the maximum velocity in the external jet leads

to a certain amplification of the temporal growth rate $\omega_{0,i}$ of the absolute mode and an increase of the absolute mode frequency $\omega_{0,r}$. However, the influence of the maximum velocity in the external jet is quite weak, which means the absolute instability conditions are determined rather by the strength of the back-flow in the external recirculation zone than the maximum velocity of the external jet.

Analogous stability calculations were carried out for the test cases characterised by the CRZ with the back-flow velocity $U_0 = -0.3$. It is known from the previous research by MICHALKE [20] and BOGUSLAWSKI and WAWRZAK [24] that such an annular jet is absolutely unstable. The current studies have aimed

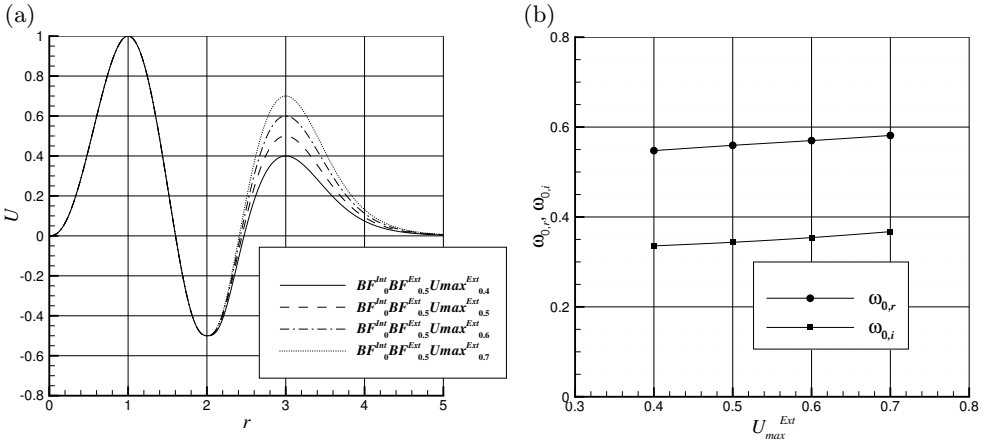


FIG. 5. Influence of the maximum velocity in the ERZ, $U_0 = 0$: (a) axial velocity profiles, (b) complex frequency of the first absolute helical mode.

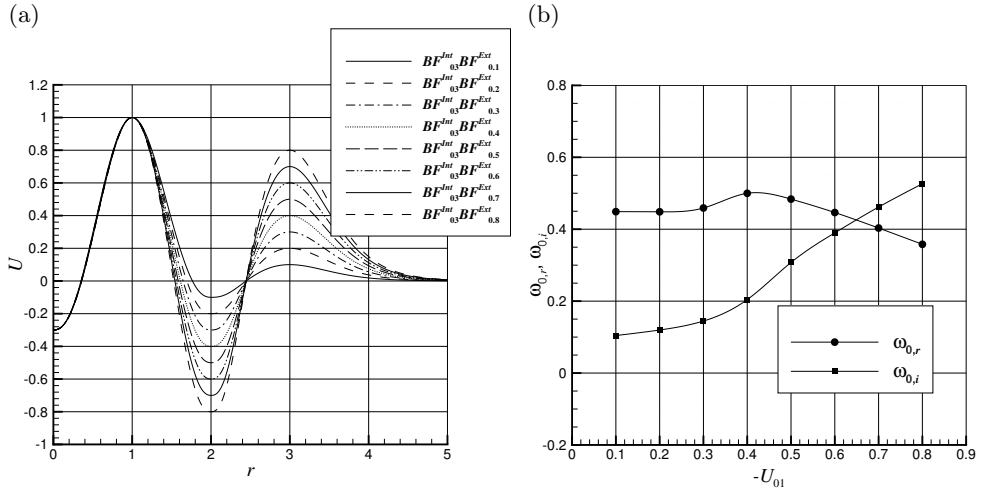


FIG. 6. Influence of the back-flow velocity in the ERZ, $U_0 = -0.3$: (a) axial velocity profiles, (b) complex frequency of the first absolute helical mode.

at an analysis of the influence of the external annular jet and the ERZ on the first helical absolutely unstable mode. The velocity profiles of all the test cases analysed with the back-flow velocity $U_0 = -0.3$ are shown in Fig. 6a and the corresponding parameters controlling the velocity profile shape are gathered in Table B.3. The influence of the back-flow strength on the first absolute helical mode is shown in Fig. 6b. The response of the absolute mode on an increasing back-flow velocity magnitude in the ERZ is in this case significantly different compared to the previous test cases with $U_0 = 0$. A weak back-flow in the ERZ has, in this case, only a slight impact on both the absolute mode growth rate $\omega_{0,i}$ and its frequency $\omega_{0,r}$. A stronger back-flow in the ERZ $U_{01} < -0.3$ leads to significant amplification of the temporal growth rate. The frequency, in turn, initially increases, attaining a maximum for $U_{01} \approx -0.4$, and then decreases along with the stronger back-flow. The evolution of the helical mode due to the ERZ is illustrated in Fig. 7 by eigenfunctions of pressure and velocity perturbations. For the back-flow velocity in the range $-0.4 < U_{01} < -0.1$ the pressure perturbations are concentrated around the shear layer between the internal jet and the CRZ at $r \approx 0.5$ while for a stronger back-flow $U_{01} < -0.4$ the maximum of the pressure perturbations is shifted to the outer shear layer formed between the internal jet and the ERZ. The velocity perturbation for a weak back-flow in the ERZ is concentrated at the jet axis. Then with increasing the back-flow magnitude a local maximum of the velocity perturbation appears at the radius corresponding to the outer shear layer. For a strong back-flow in the ERZ $U_{01} < -0.5$, for which the absolute mode growth rate is amplified, the velocity perturbation eigenfunction is characterised by three local maxima: at the jet axis, around the inner and outer shear layers of the internal jet.

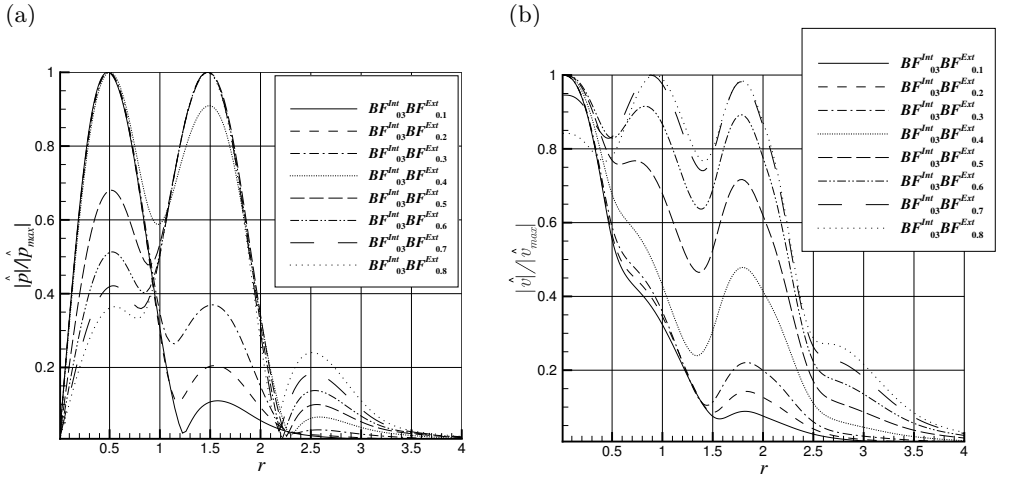


FIG. 7. Influence of the back-flow velocity in the ERZ on eigenfunctions of the first helical absolute mode, $U_0 = -0.3$: (a) pressure perturbation, (b) velocity perturbation.

Again, the influence of the maximum velocity in the external jet was studied for a fixed back-flow velocity in the ERZ. The velocity profiles analysed for the test cases with $U_0 = -0.3$ and $U_{01} = -0.5$ and changing the maximum velocity in the external jet are shown in Fig. 8a and corresponding parameters of the external jet are presented in Table B.6. An impact of the maximum velocity in the external jet on the absolutely unstable helical mode is shown in Fig. 8b. It is seen that the response of both the temporal growth rate $\omega_{0,i}$ and the absolute mode frequency $\omega_{0,r}$ to a varying maximum velocity of the external jet is quite weak as already observed for the jet with $U_0 = 0$.

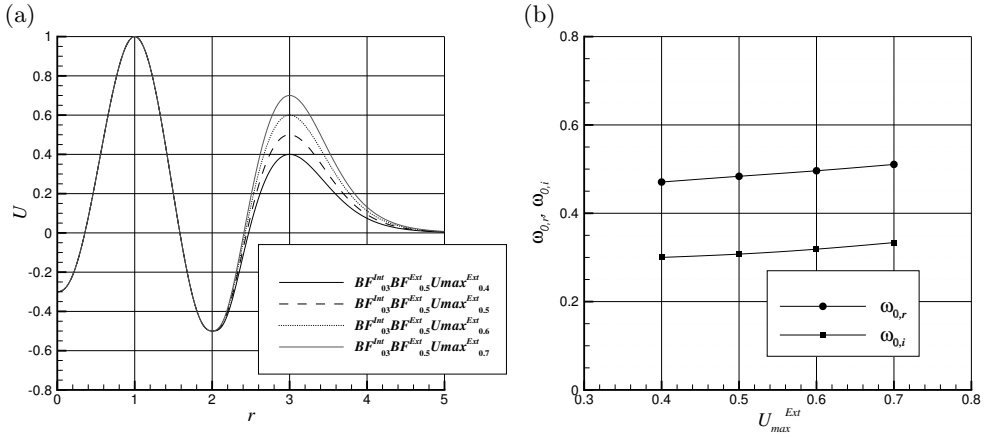


FIG. 8. Influence of the maximum velocity in the ERZ, $U_0 = -0.3$: (a) axial velocity profiles, (b) complex frequency of the first absolute helical mode.

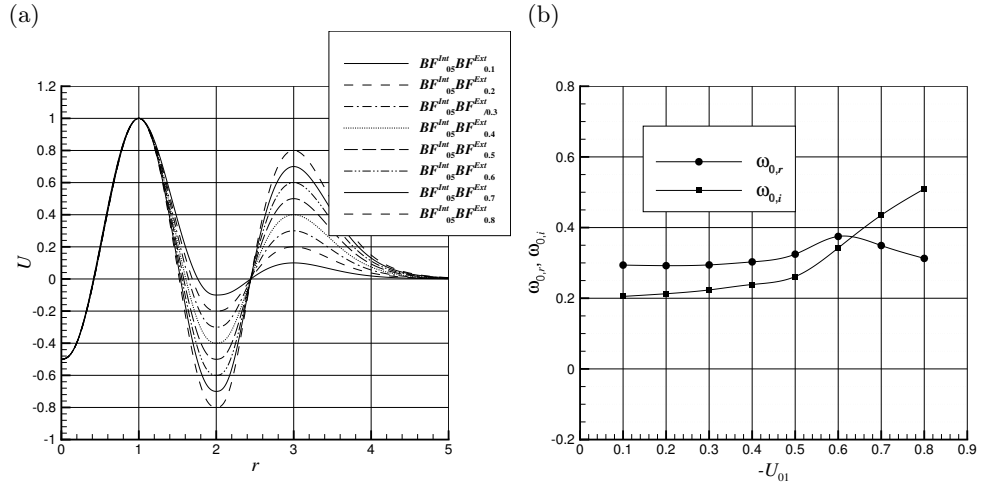


FIG. 9. Influence of the back-flow velocity in the ERZ, $U_0 = -0.5$: (a) axial velocity profiles, (b) complex frequency of the first absolute helical mode.

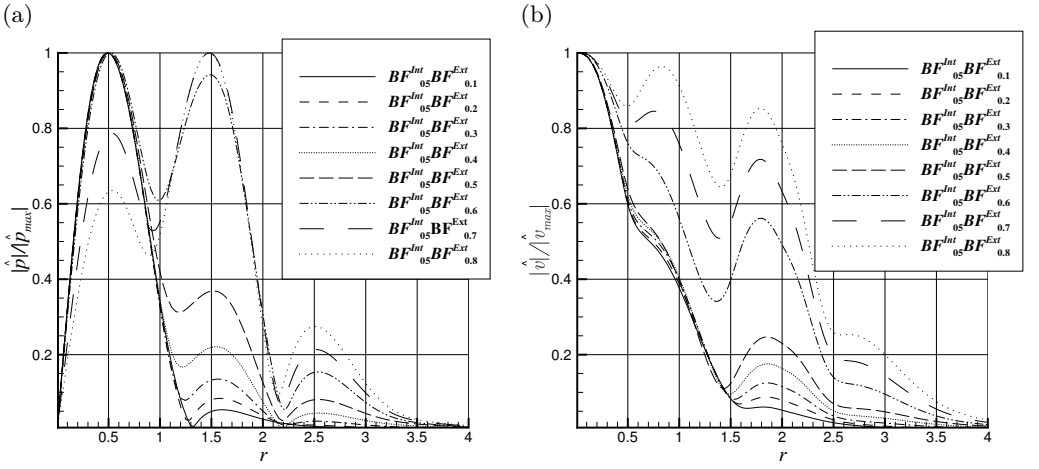


FIG. 10. Influence of the back-flow velocity in the ERZ on eigenfunctions of the first helical absolute mode, $U_0 = -0.5$: (a) pressure perturbation, (b) velocity perturbation.

Finally, the influence of the ERZ on the jet stability with the back-flow $U_0 = -0.5$ in the CRZ was studied. The axial velocity profiles and the complex frequency of the first helical absolute mode for this case are shown in Fig. 9. An interesting observation is that a weak impact on the jet stability is in this case reported for a wider range of the back-flow $-0.5 < U_{01} < -0.1$. The temporal growth rate of the absolute mode is significantly amplified for $U_{01} < -0.5$. Taking into account both cases for different back-flow velocities in the CRZ zone one could conclude that an influence of the back-flow in the ERZ is revealed only when the back-flow in the ERZ exceeds the back-flow in the CRZ. Similarly to the previous case, the amplified growth rate $\omega_{0,i}$ as a function of the back-flow in

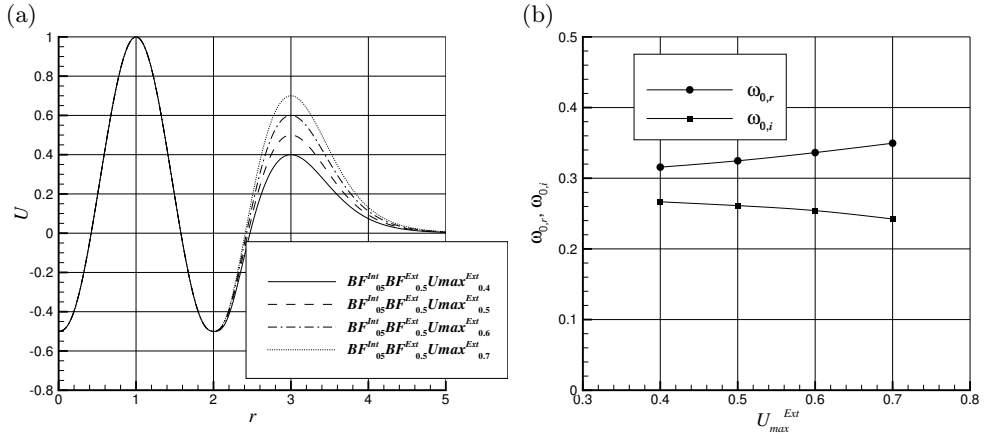


FIG. 11. Influence of the maximum velocity in the ERZ, $U_0 = -0.5$: (a) axial velocity profiles, (b) complex frequency of the first absolute helical mode.

the ERZ is associated with initially increased the absolute mode frequency $\omega_{0,r}$ which further drops down along with the stronger back-flow. An evolution of the eigenfunctions along with the growing back-flow in the ERZ, shown in Fig. 10, seems to be analogous to the previous case with qualitative changes of the perturbation distribution observed when the back-flow velocity exceeds $U_{01} = -0.5$.

Figure 11 presents influence of the maximum velocity in the external jet on the complex frequency. As in the previous cases an increase of the maximum velocity in the external jet is associated with a weak increase of the helical mode frequency $\omega_{0,r}$, but contrary to the previous results, for $U_0 = -0.5$, a slight decrease of the absolute mode growth rate $\omega_{0,i}$ is observed.

### 4.2. Swirling jets

In practical applications of double annular jets in combustion chambers, mixing of fuel and oxidiser is enhanced and the flame is stabilised by the use of swirl applied to the internal or external jet. Hence, the stability analysis was completed for swirling jets. Using the previous results for swirling single annular jet [24] only an influence of the swirling degree for the internal and external jets was analysed assuming that other parameters of the tangential velocity profiles had a minor influence on the stability characteristics. In all the calculations for swirling jets the parameters defining the tangential velocity profiles in the internal and external jets were as follows:

$$N_W^{int} = N_W^{ext} = 5, \quad R_{W_{max}}^{int} = 1, \quad R_{W_{max}}^{ext} = 3. \tag{4.1}$$

The swirl degrees were varying in ranges $A^{int} = 0 - 0.9$ and $A^{ext} = 0 - 0.9$. The tangential velocity profiles used in the calculations are shown in Fig. 12.

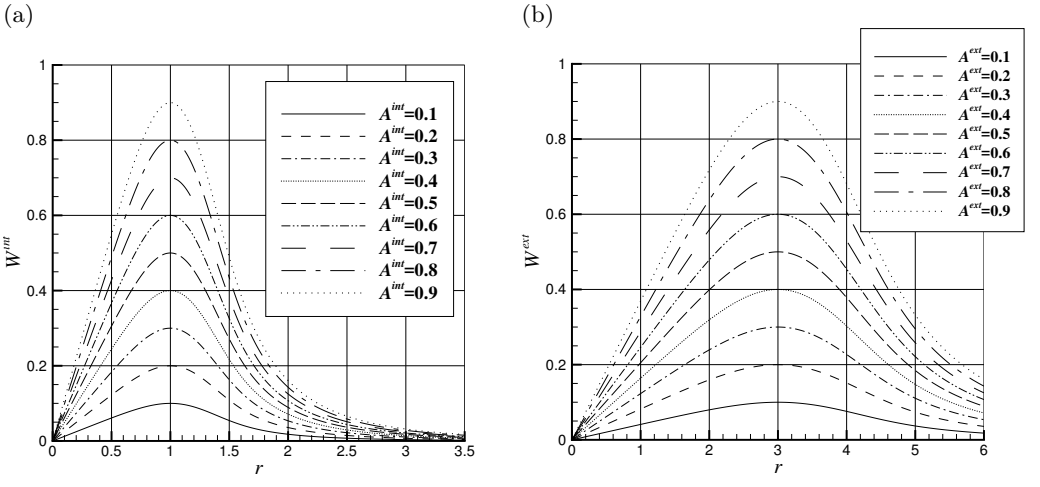


FIG. 12. Tangential velocity profiles: (a) internal jet, (b) external jet.

An influence of the swirling was analysed for the following test cases: $BF_0^{int}BF_{03}^{ext}$, $BF_0^{int}BF_{06}^{ext}$, $BF_{03}^{int}BF_{03}^{ext}$, $BF_{03}^{int}BF_{06}^{ext}$, $BF_{05}^{int}BF_{03}^{ext}$, $BF_{05}^{int}BF_{06}^{ext}$. In each test case the swirl degree of the internal or external jets was varying in a wide range. Figure 13 shows an influence of the swirling in the internal and external jets for the flow without the CRZ ($U_0 = 0$). Such double annular jets are absolutely unstable provided that a back-flow in the external jet is strong enough. In both the cases analysed $BF_0^{int}BF_{03}^{ext}$ and $BF_0^{int}BF_{06}^{ext}$ the first helical mode is absolutely unstable. An influence of the swirl imposed on the internal jet is shown in Fig. 13a. It is seen that a swirl of the internal jet only slightly affects the first absolute mode frequency $\omega_{0,r}$ and the temporal growth rate $\omega_{0,i}$. For both back-flow velocities in the external jet, $U_{01} = -0.3$ and $U_{01} = -0.6$, swirling in the internal jet causes an increase of the absolute mode frequency $\omega_{0,r}$. For $U_{01} = -0.3$ a limited swirl increases the growth rate and a stronger swirl leads to a smaller growth rate $\omega_{0,i}$. In the case of a stronger back-flow in the external jet, $U_{01} = -0.6$, a swirling in the internal jet leads to a decrease of the growth rate. A swirl of the external jet, the influence of which is shown in Fig. 13b, for both back-flow velocities $U_{01} = -0.3$ and $U_{01} = -0.6$, causes the increase of the absolute mode frequency but the growth rate is significantly damped. It is seen that for $U_{01} = -0.3$, swirling with a degree $A^{ext} > 0.5$ leads to the helical mode suppression. Further, an influence of the swirl on the eigenfuctions of pressure and velocity perturbations is analysed for the test cases shown in Fig. 13. Figure 14 shows influence of the swirling of the internal jet on the perturbation amplitude in the test case $BF_0^{int}BF_{03}^{ext}$. It is seen that the swirling degree $A^{int} = 0.4$, for which the maximum of the growth rate is observed, increases the perturbation level in

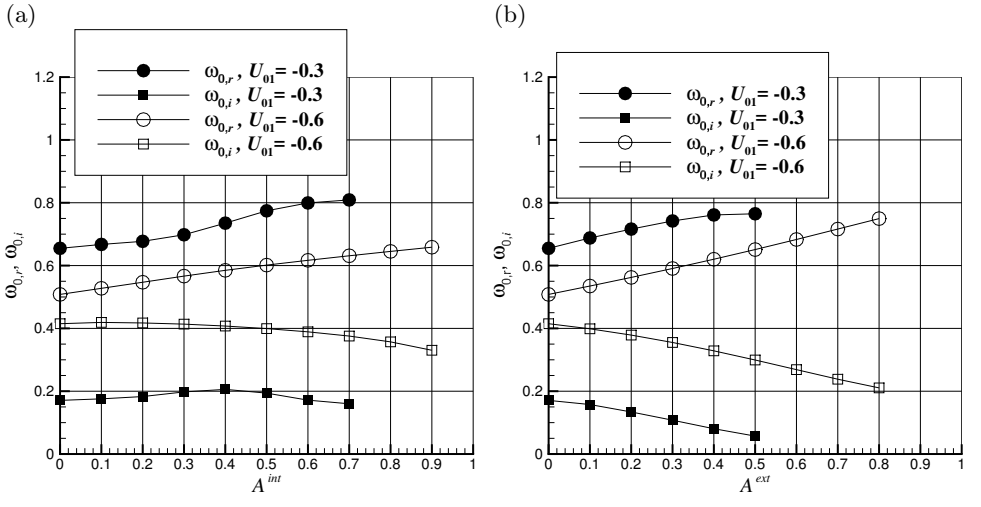


FIG. 13. Influence of the swirl degree on the complex frequency of the first absolute helical mode, $U_0 = 0$: (a) swirling of internal jet, (b) swirling of external jet.

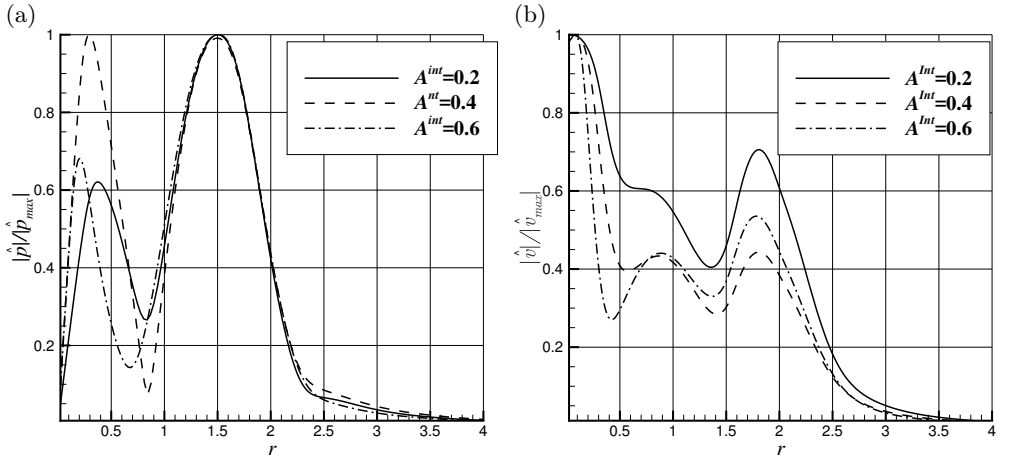


FIG. 14. Influence of the swirling degree of the internal jet on eigenfunctions of the first helical absolute mode, $U_0 = 0$, $U_{01} = -0.3$: (a) pressure perturbation, (b) velocity perturbation.

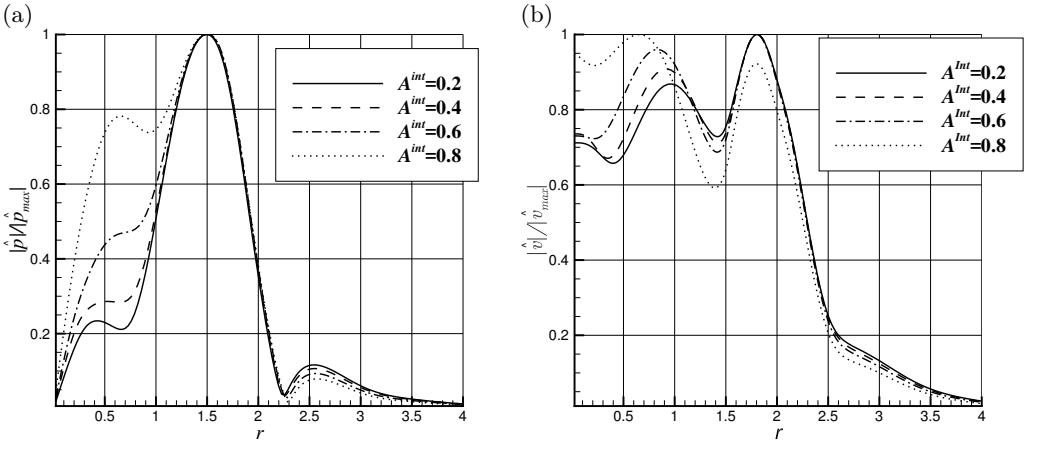


FIG. 15. Influence of the swirl degree of the internal jet on eigenfunctions of the first helical absolute mode, $U_0 = 0$, $U_{01} = -0.6$: (a) pressure perturbation, (b) velocity perturbation.

the region closer to the jet axis and for a higher swirl again the perturbation level is intensified at the jet periphery. In the case of higher back-flow in the external jet $BF_0^{int}BF_{06}^{ext}$, shown in Fig. 15, a monotonic growth of the perturbation amplitude in the region of the internal jet is observed. Despite that the swirling of the internal jet does not promote the absolutely unstable mode in this case, swirling can control the location of the perturbation development. As shown in Fig. 13 swirling of the external jet decreases the growth rate leading even to suppression of the absolute mode. However, Figs. 16 and 17 show that even though the max-

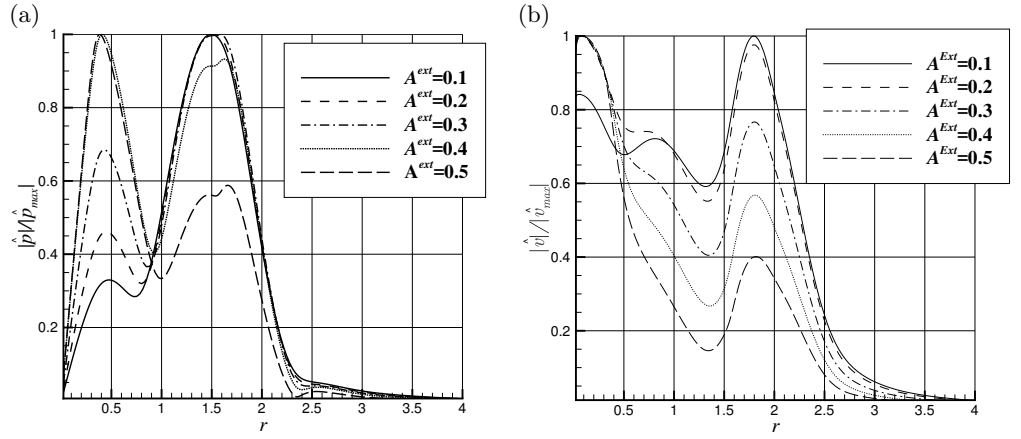


FIG. 16. Influence of the swirl degree of the external jet on eigenfunctions of the first helical absolute mode, $U_0 = 0$, $U_{01} = -0.3$: (a) pressure perturbation, (b) velocity perturbation.

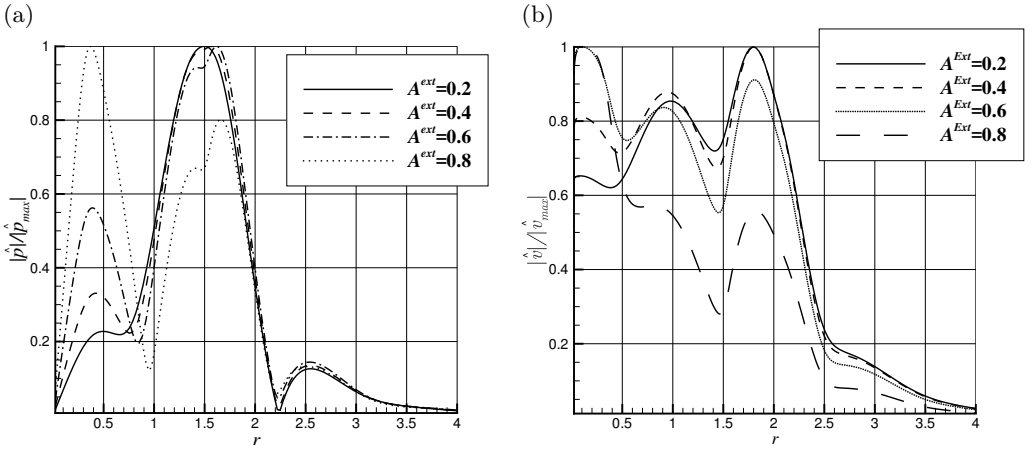


FIG. 17. Influence of the swirl degree of the external jet on eigenfunctions of the first helical absolute mode, $U_0 = 0$, $U_{01} = -0.6$: (a) pressure perturbation, (b) velocity perturbation.

imum velocity of tangential velocity is located at the centre of the ERZ, swirling in these cases leads to a shift of the perturbation maximum to the jet centre.

Further analysis refers to the test cases with the back-flow in the CRZ. An influence of the swirl on the complex frequency of the test cases $BF_{03}^{int}BF_{03}^{ext}$ and $BF_{03}^{int}BF_{06}^{ext}$ is presented in Fig. 18. A swirl of the internal jet in these cases affects the frequency $\omega_{0,r}$ and the growth rate $\omega_{0,i}$ of the first helical absolutely unstable mode in a manner similar to that observed for the single annular jet as shown by BOGUSLAWSKI and WAWRZAK [24]. A limited amount of swirl promotes the absolute mode with a maximum of the growth rate observed

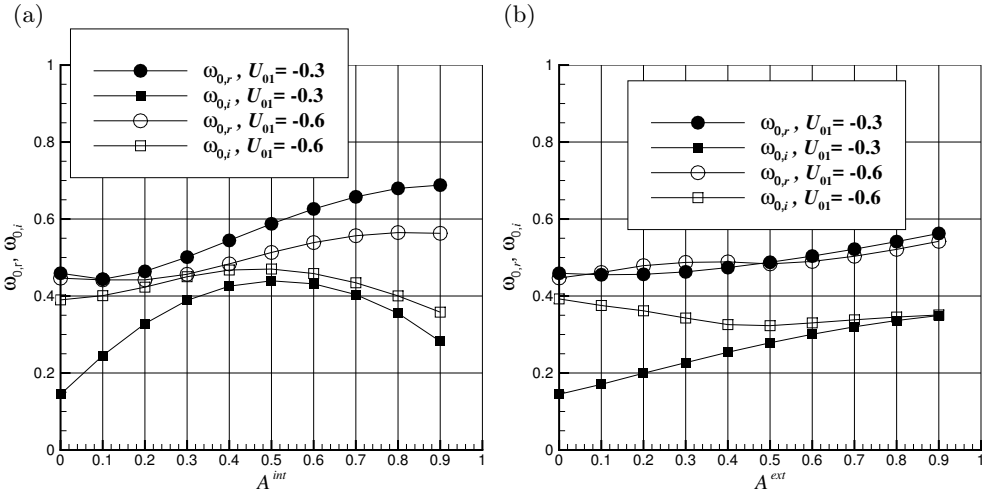


FIG. 18. Influence of the swirl degree on the complex frequency of the first absolute helical mode, $U_0 = -0.3$: (a) swirling of internal jet, (b) swirling of external jet.

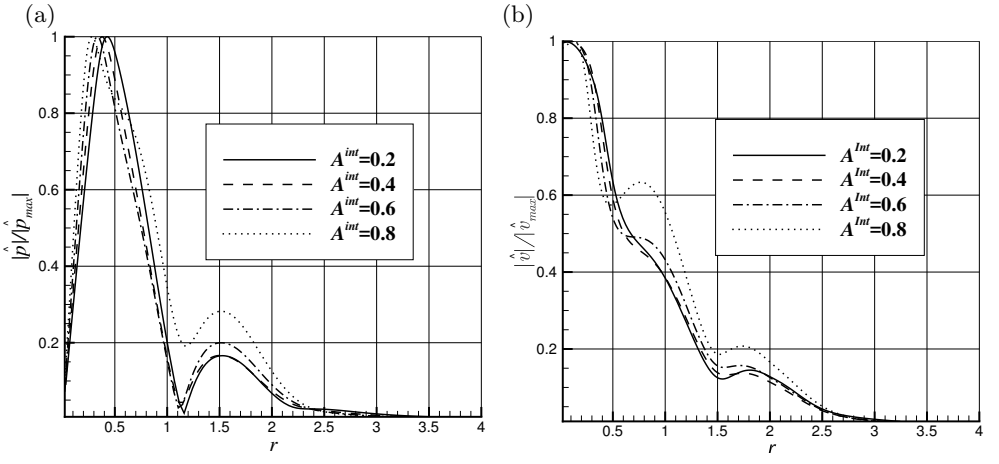


FIG. 19. Influence of the swirl degree of the internal jet on eigenfunctions of the first helical absolute mode, $U_0 = -0.3$, $U_{01} = -0.3$: (a) pressure perturbation, (b) velocity perturbation.

for $A^{int} \approx 0.5$. A monotonic growth of the absolute frequency $\omega_{0,r}$ as a function of the swirling degree is observed. For a higher back-flow velocity in the ERZ for $U_{01} = -0.6$ influence of the swirl on the frequency is weaker. By contrast, swirling of the external jet leads to a monotonic increase of the absolute mode growth rate in the case of the lower back-flow $U_{01} = -0.3$ and slight damping for the higher back-flow velocity $U_{01} = -0.6$. The internal jet swirling affects weakly the pressure and velocity eigenfunctions in the case of $U_{01} = -0.3$ as shown in Fig. 19. The pressure perturbation maximum is moving to the jet axis and some

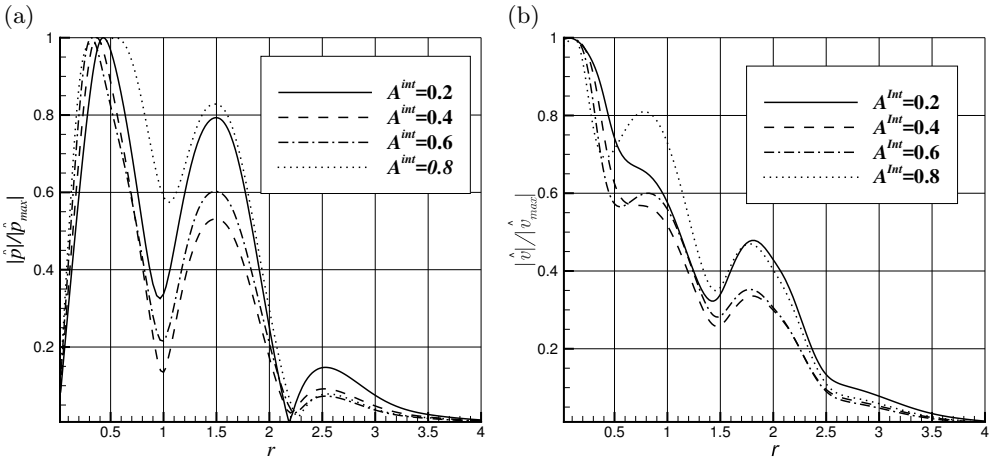


FIG. 20. Influence of the swirl degree of the internal jet on eigenfunctions of the first helical absolute mode, $U_0 = -0.3$, $U_{01} = -0.6$: (a) pressure perturbation, (b) velocity perturbation.

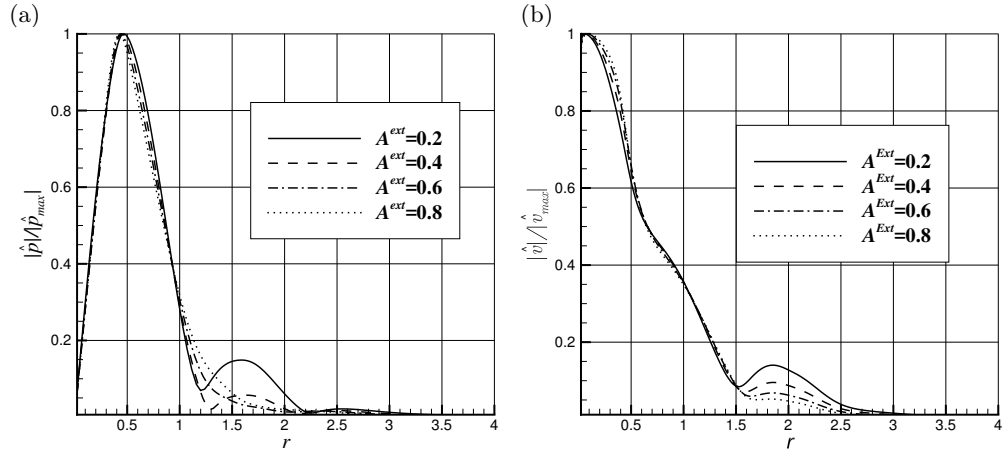


FIG. 21. Influence of the swirl degree of the external jet on eigenfunctions of the first helical absolute mode, $U_0 = -0.3$, $U_{01} = -0.3$: (a) pressure perturbation, (b) velocity perturbation.

growth is observed in the outer shear layer of the internal jet as a function of the swirling degree. The velocity perturbation is also slightly growing in the inner shear layer of the internal jet compared to the perturbation maximum located at the jet axis. A stronger influence of the swirling of the internal jet is observed for the back-flow velocity $U_{01} = -0.6$ shown in Fig. 20. Quite a similar influence of the external jet swirl on the pressure and velocity perturbation eigenfunctions is observed in Figs. 21 and 22. Again, in the case of the weaker back-flow velocity $U_{01} = -0.3$, the influence of the swirl is weak and much stronger for the higher back-flow magnitude.

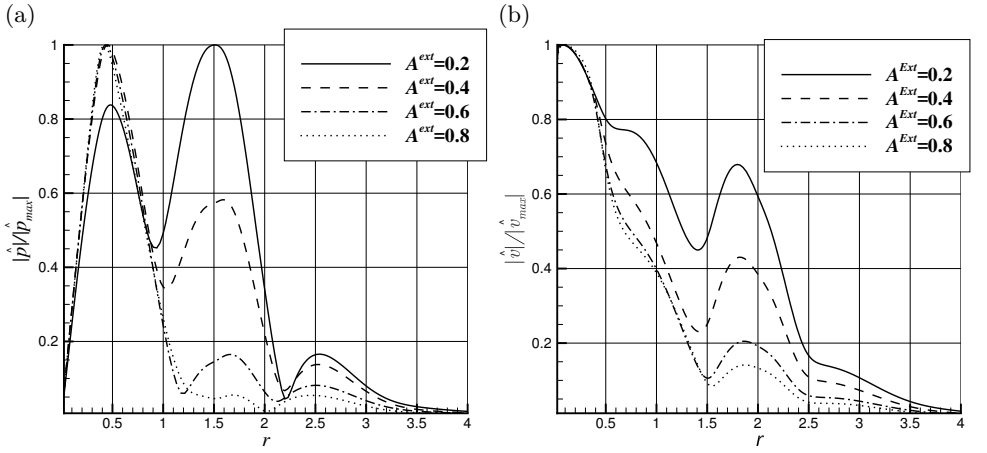


FIG. 22. Influence of the swirl degree of the external jet on eigenfunctions of the first helical absolute mode, $U_0 = -0.3$, $U_{01} = -0.6$: (a) pressure perturbation, (b) velocity perturbation.

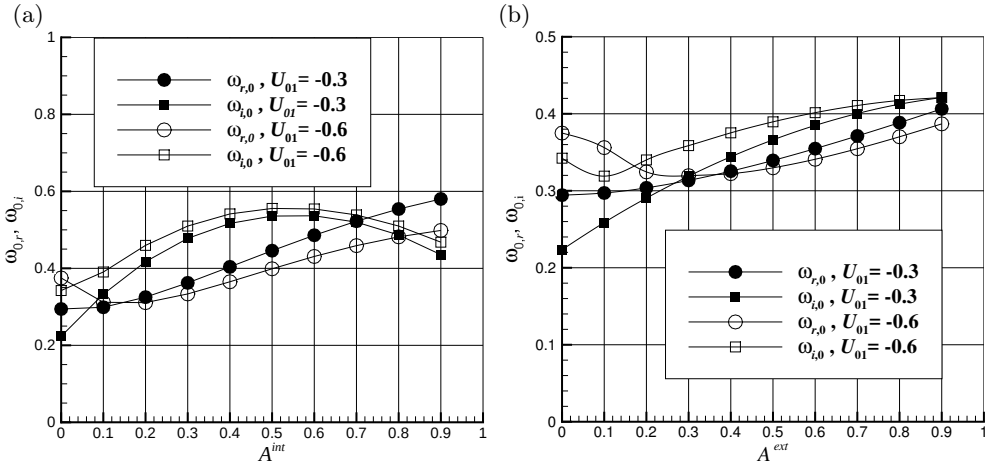


FIG. 23. Influence of the swirl degree on the complex frequency of the first absolute helical mode, $U_0 = -0.5$: (a) swirling of internal jet, (b) swirling of external jet.

Finally, the test cases with the strongest back-flow $U_0 = -0.5$ in the CRZ were analysed. Figure 23 shows a swirl influence on the complex frequency of the first helical mode for the test cases $BF_{05}^{int}BF_{03}^{ext}$ and $BF_{05}^{int}BF_{06}^{ext}$. One can see that also in this case a limited amount of the internal jet swirl promotes the absolutely unstable first helical mode. The maximum of the growth rate $\omega_{0,i}$ in both the cases analysed is for the swirling degree $A^{int} \approx 0.5$. Swirling of the internal jet leads to an increase in the absolute mode frequency $\omega_{0,r}$. Swirling of the external jet, in the case $U_{01} = -0.3$, causes an increase of both the absolute mode frequency and the growth rate while for the stronger back-flow in the ERZ a weak swirl leads to a slight decrease of the frequency and the growth rate and

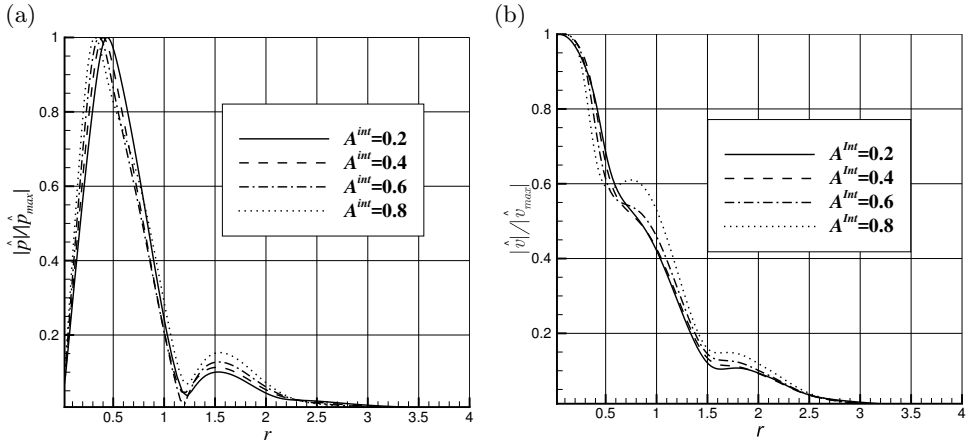


FIG. 24. Influence of the swirl degree of the internal jet on eigenfunctions of the first helical absolute mode, $U_0 = -0.5$, $U_{01} = -0.3$: (a) pressure perturbation, (b) velocity perturbation.

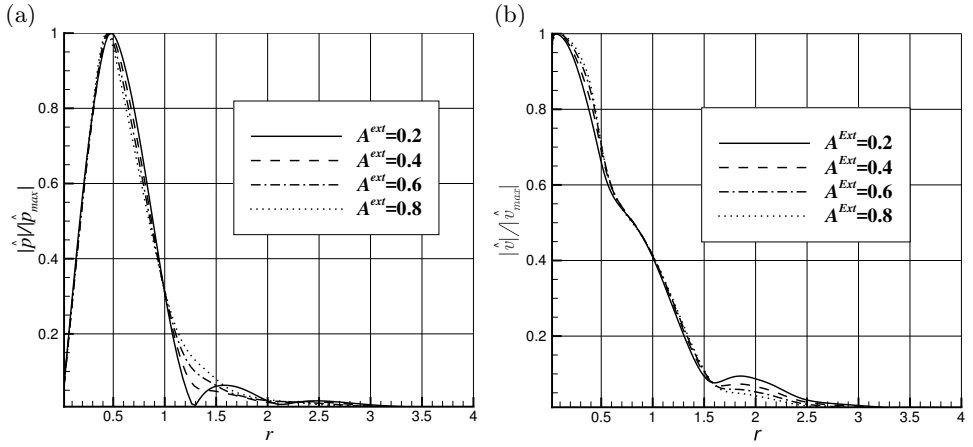


FIG. 25. Influence of the swirl degree of the external jet on eigenfunctions of the first helical absolute mode, $U_0 = -0.5$, $U_{01} = -0.3$: (a) pressure perturbation, (b) velocity perturbation.

a stronger swirl increases the frequency and the growth rate. In the case of the strongest back-flow in the CRZ, the perturbations are located in this zone and the swirl of the internal jet very weakly affects the eigenfunctions, as shown in Fig. 24. Similarly, the swirl of the external jet very weakly influences perturbation distribution for $U_0 = -0.5$ shown in Fig. 25. The influence of the swirl of the internal and external jets is also weak in the case of stronger back-flow in the ERZ $U_{01} = -0.6$ (not shown in the paper). One can conclude that if the back-flow in the CRZ is strong enough the first helical mode is triggered in this zone and a swirl can influence the perturbation frequency and the growth rate with a very weak impact on perturbation amplitude distribution across the jet.

## 5. Conclusions

The paper presented the local stability analysis of the double annular non-swirling and swirling jets. The calculations showed that in the case of the non-swirling jet the first absolutely unstable helical mode can be triggered by a back-flow in the CRZ or the ERZ. For the test cases without the back-flow in the CRZ, a relatively weak back-flow in the ERZ led to the absolute instability of the first helical mode. By contrast, for a sufficiently strong back-flow in the CRZ, the instability characteristics were affected by the ERZ only if the back-flow was stronger than the one in the CRZ. The increased growth rate by the back-flow in the ERZ was associated with a decrease of the absolute mode frequency. The maxima of the perturbations triggered by the absolute mode are located close to the jet axis if the flow instability is controlled by the back-flow in the CRZ or in the region of the ERZ in all the cases in which the absolute mode is triggered by the back-flow in this zone. The influence of the swirl in the internal or external jet was studied for chosen test cases. When the absolute mode was generated by the back-flow in the ERZ without back-flow in the CRZ, the influence of the swirl in the internal jet was very weak, while the swirl of the external jet resulted in the increased frequency and the decreased growth rate. If the flow was dominated by the back-flow in the CRZ, a limited swirl of the internal jet promoted the absolute mode growth rate with the maximum for $A^{int} \approx 0.5$. The frequency of the helical mode was growing along with the swirling degree of the internal jet. The influence of the swirl in the external jet depended on a relation between the strength of the back-flows in the CRZ and ERZ. Swirling affected also the shape of the eigenfunctions of the first helical mode. In general, the influence of the swirl was stronger for the flow without back-flow in the CRZ and weaker when the flow was controlled by this back-flow.

## Appendix A. Procedures for calculating the base flow parameters

The obvious constraints for such a velocity profile are as follows:

$$\left.\frac{dU^{int}}{dr}\right|_{r=0} = 0, \qquad \left.\frac{dU^{int}}{dr}\right|_{r=R_{01}} = 0,$$
$$\left.\frac{dU^{ext}}{dr}\right|_{r=R_{01}} = 0, \qquad \left.\frac{dU^{ext}}{dr}\right|_{r=\infty} = 0. \tag{A.1}$$

It can easily be verified that the function describing the axial velocity profile satisfies these constraints.

If the radius tends to zero then

$$\begin{aligned}(A.2)\qquad \lim_{r\to 0} U^{int}(r) &= U_{in}^{int}\tanh(-b_{in}^{int}R_{in}^{int}) - U_{out}^{int}\tanh(-b_{out}^{int}R_{out}^{int})\\ &+ \frac{b_{in}^{int}U_{in}^{int}}{\cosh^2(-b_{in}^{int}R_{in}^{int})b_{in}^{0,int}} - \frac{b_{out}^{int}U_{out}^{int}}{\cosh^2(-b_{out}^{int}R_{out}^{int})b_{out}^{0,int}}\\ &- \frac{b_{in}^{int}U_{in}^{int}}{\cosh^2[b_{in}^{int}(R_{01}-R_{in}^{int})]}\,\frac{[1-\tanh(b_{in}^{0,int}R_{01})]}{b_{in}^{0,int}}\\ &+ \frac{b_{out}^{int}U_{out}^{int}}{\cosh^2[b_{out}^{int}(R_{01}-R_{out}^{int})]}\,\frac{[1-\tanh(b_{out}^{0,int}R_{01})]}{b_{out}^{0,int}}\\ &- U_{in}^{int} + U_{out}^{int} + U_{\infty}^{int} = U_0.\end{aligned}$$

As $U_0$ is imposed as a parameter there is a relation between $U_{in}^{int}$ and $U_{out}^{int}$. Assuming a certain value for $U_{in}^{int}$ the parameter $U_{out}^{int}$ is expressed as

$$(A.3)\qquad U_{out}^{int} = \frac{U_{in}^{int}L_{in}^{int} - U_0 + U_{\infty}^{int}}{L_{out}^{int}},$$

where

$$\begin{aligned}(A.4)\qquad L_{in}^{int} =\ & \tanh(-b_{in}^{int}R_{in}^{int}) + \frac{b_{in}^{int}}{\cosh^2(-b_{in}^{int}R_{in}^{int})b_{in}^{0,int}}\\ &- \frac{b_{in}^{int}}{\cosh^2[b_{in}^{int}(R_{01}-R_{in}^{int})]}\,\frac{[1-\tanh(b_{in}^{0,int}R_{01})]}{b_{in}^{0,int}} - 1,\end{aligned}$$

$$\begin{aligned}(A.5)\qquad L_{out}^{int} =\ & \tanh(-b_{out}^{int}R_{out}^{int}) + \frac{b_{out}^{int}}{\cosh^2(-b_{out}R_{out}^{int})b_{out}^{0,int}}\\ &+ \frac{b_{out}^{int}}{\cosh^2[b_{out}^{int}(R_{01}-R_{out}^{int})]}\,\frac{[1-\tanh(b_{0,out}^{int}R_{01})]}{b_{0,out}^{int}} - 1.\end{aligned}$$

The $U_{\infty}^{int}$ parameter is used to obtain the presumed back flow velocity $U_{01}$ in the ERZ for $r = R_{01}$

$$\begin{aligned}(A.6)\quad U_{\infty}^{int} &= U_{01} - U_{in}^{int}\tanh[b_{in}^{int}(R_{01}-R_{in}^{int})]\\ &+ U_{out}^{int}\tanh[b_{out}^{int}(R_{01}-R_{out}^{int})]\\ &- \frac{b_{in}^{int}U_{in}^{int}}{\cosh^2(-b_{in}^{int}R_{in}^{int})}\,\frac{[1-\tanh(b_{in}^{0,int}R_{01})]}{b_{in}^{0,int}}\\ &+ \frac{b_{out}^{int}U_{out}^{int}}{\cosh^2(-b_{out}^{int}R_{out}^{int})}\,\frac{[1-\tanh(b_{out}^{0,int}R_{01})]}{b_{out}^{0,int}}\\ &+ \frac{b_{in}^{int}U_{in}^{int}}{\cosh^2[b_{in}^{int}(R_{01}-R_{in}^{int})]}\,\frac{1}{b_{in}^{0,int}} - \frac{b_{out}^{int}U_{out}^{int}}{\cosh^2[b_{out}^{int}(R_{01}-R_{out}^{int})]}\,\frac{1}{b_{out}^{0,int}}\\ &+ U_{in}^{int} - U_{out}^{int}.\end{aligned}$$

Velocity gradients in inner and outer shear layers are controlled by $b_{in}^{int}$ and $b_{out}^{int}$ parameters, respectively. The parameter $U_{in}^{int}$ is chosen in order to get a presumed maximum value of the axial velocity $U_{max}^{int} = 1$. Varying $b_{in}^{int}$-coefficient $R_{out}^{int}$ is kept constant while $R_{in}^{int}$ is calculated to obtain the maximum of the velocity at a chosen radius $R_{U_{max}}^{int} = 1$. Conversely, varying $b_{out}^{int}$ the $R_{in}^{int}$ is fixed while $R_{out}^{int}$ is calculated to obtain the maximum of the velocity at a chosen radius $R_{U_{max}}^{int} = 1$. The required parameters are obtained by Newton's procedure [33].

Further the velocity profile is continued accross the external jet starting from the radius $R_{01}$ with the function $U^{ext}(r)$. Apart from the zero gradient at the $R_{01}$ the velocity in the ERZ must be equal to the presumed back-flow velocity $U_{01}$

$$U^{ext}(R_{01}) = U^{int}(R_{01}) = U_{01}. \tag{A.7}$$

Hence,

$$\begin{aligned} U^{ext}(R_{01}) = {} & U_{in}^{ext} \tanh[b_{in}^{ext}(R_{01} - R_{in}^{ext})] \\ & - U_{out}^{ext} \tanh[b_{out}^{ext}(R_{01} - R_{out}^{ext})] \\ & \frac{b_{in}^{ext} U_{in}^{ext}}{\cosh^2[b_{in}^{ext}(R_{01} - R_{in}^{ext})]} \frac{1}{b_{in}^{0,ext}} \\ & - \frac{b_{out}^{ext} U_{out}^{ext}}{\cosh^2[b_{out}^{ext}(R_{01} - R_{out}^{ext})]} \frac{1}{b_{out}^{0,ext}} \\ & - U_{in}^{ext} + U_{out}^{ext} = U_{01}. \end{aligned} \tag{A.8}$$

As $U_{01}$ is the presumed parameter of the velocity profile it gives a relation between $U_{in}^{ext}$ and $U_{out}^{ext}$

$$U_{out}^{ext} = \frac{U_{in}^{ext} L_{in}^{ext} - U_{01}}{L_{out}^{ext}}, \tag{A.9}$$

where

$$L_{in}^{ext} = \tanh[b_{in}^{ext}(R_{01} - R_{in}^{ext})] + \frac{b_{in}^{ext}}{\cosh^2[b_{in}^{ext}(R_{01} - R_{in}^{ext})] b_{in}^{0,ext}} - 1, \tag{A.10}$$

$$L_{out}^{ext} = \tanh[b_{out}^{ext}(R_{01} - R_{out}^{ext})] + \frac{b_{out}^{ext}}{\cosh^2[b_{out}^{ext}(R_{01} - R_{out}^{ext})] b_{out}^{0,ext}} - 1. \tag{A.11}$$

All other parameters for the external annular jet are calculated in an analogous way as for the internal one.

## Appendix B. Tables with the base flow parameters

**Table B.1. List of the parameters of the axial velocity profiles for $U_0 = 0$.**

Internal annular jet

| Test case | $R_{out}^{int}$ | $U_{in}^{int}$ | $U_{out}^{int}$ | $U_\infty$ | $U_0$ |
|---|---|---|---|---|---|
| $BF_0^{int}BF_{01}^{ext}$ | 1.2908 | 2.0222 | 2.1198 | −0.6927 | 0 |
| $BF_0^{int}BF_{02}^{ext}$ | 1.3289 | 1.9619 | 2.1612 | −0.8899 | 0 |
| $BF_0^{int}BF_{03}^{ext}$ | 1.3646 | 1.9136 | 2.2191 | −1.0970 | 0 |
| $BF_0^{int}BF_{04}^{ext}$ | 1.3985 | 1.8740 | 2.2908 | −1.3152 | 0 |
| $BF_0^{int}BF_{05}^{ext}$ | 1.4309 | 1.8410 | 2.3748 | −1.5455 | 0 |
| $BF_0^{int}BF_{06}^{ext}$ | 1.4621 | 1.8130 | 2.4703 | −1.7892 | 0 |
| $BF_0^{int}BF_{07}^{ext}$ | 1.4922 | 1.7889 | 2.5770 | −2.0479 | 0 |
| $BF_0^{int}BF_{08}^{ext}$ | 1.5215 | 1.7680 | 2.6951 | −2.3232 | 0 |

External annular jet

| Test case | $R_{in}^{ext}$ | $U_{max}^{ext}$ | $U_{in}^{ext}$ | $U_{out}^{ext}$ | $U_{01}$ |
|---|---|---|---|---|---|
| $BF_0^{int}BF_{01}^{ext}$ | 2.1556 | 0.1 | 0.3623 | 0.1128 | −0.1 |
| $BF_0^{int}BF_{02}^{ext}$ | 2.1556 | 0.2 | 0.7245 | 0.2256 | −0.2 |
| $BF_0^{int}BF_{03}^{ext}$ | 2.1556 | 0.3 | 1.0868 | 0.3384 | −0.3 |
| $BF_0^{int}BF_{04}^{ext}$ | 2.1557 | 0.4 | 1.4490 | 0.4512 | −0.4 |
| $BF_0^{int}BF_{05}^{ext}$ | 2.1557 | 0.5 | 1.8113 | 0.5641 | −0.5 |
| $BF_0^{int}BF_{06}^{ext}$ | 2.1557 | 0.6 | 2.1736 | 0.6769 | −0.6 |
| $BF_0^{int}BF_{07}^{ext}$ | 2.1557 | 0.7 | 2.5358 | 0.7897 | −0.7 |
| $BF_0^{int}BF_{08}^{ext}$ | 2.1557 | 0.8 | 2.8981 | 0.9025 | −0.8 |

**Table B.2. List of the parameters of the axial velocity profiles for $U_0 = 0$, $U_{01} = -0.5$, varying $U_{max}^{ext}$.**

External annular jet

| Test case | $R_{in}^{ext}$ | $U_{max}^{ext}$ | $U_{in}^{ext}$ | $U_{out}^{ext}$ | $U_{01}$ |
|---|---|---|---|---|---|
| $BF_0^{int}BF_{05}^{ext}Umax_{04}^{ext}$ | 1.9924 | 0.4 | 2.2072 | 0.4449 | −0.5 |
| $BF_0^{int}BF_{05}^{ext}Umax_{06}^{ext}$ | 2.2325 | 0.6 | 1.8082 | 0.6836 | −0.5 |
| $BF_0^{int}BF_{05}^{ext}Umax_{07}^{ext}$ | 2.2826 | 0.7 | 1.8831 | 0.8038 | −0.5 |

**Table B.3. List of the parameters of the axial velocity profiles for $U_0 = -0.3$.**

Internal annular jet

| Test case | $R_{out}^{int}$ | $U_{in}^{int}$ | $U_{out}^{int}$ | $U_\infty$ | $U_0$ |
|---|---|---|---|---|---|
| $BF_{03}^{int}BF_{01}^{ext}$ | 1.1800 | 2.9545 | 2.7672 | −0.60144 | −0.3 |
| $BF_{03}^{int}BF_{02}^{ext}$ | 1.2163 | 2.8280 | 2.7333 | −0.77579 | −0.3 |
| $BF_{03}^{int}BF_{03}^{ext}$ | 1.3646 | 2.7291 | 2.7291 | −0.95622 | −0.3 |
| $BF_{03}^{int}BF_{04}^{ext}$ | 1.2817 | 2.6496 | 2.7469 | −1.1431 | −0.3 |
| $BF_{03}^{int}BF_{05}^{ext}$ | 1.3116 | 2.5843 | 2.7818 | −1.3370 | −0.3 |
| $BF_{03}^{int}BF_{06}^{ext}$ | 1.3401 | 2.5297 | 2.8306 | −1.5382 | −0.3 |
| $BF_{03}^{int}BF_{07}^{ext}$ | 1.3673 | 2.4834 | 2.8914 | −1.7474 | −0.3 |
| $BF_{03}^{int}BF_{08}^{ext}$ | 1.3934 | 2.4435 | 2.9626 | −1.9651 | −0.3 |

**Table B.3. [cont.]**

External annular jet

| Test case | $R_{in}^{ext}$ | $U_{max}^{ext}$ | $U_{in}^{ext}$ | $U_{out}^{ext}$ | $U_{01}$ |
|---|---|---|---|---|---|
| $BF_{03}^{int}BF_{01}^{ext}$ | 2.1556 | 0.1 | 0.3623 | 0.1128 | −0.1 |
| $BF_{03}^{int}BF_{02}^{ext}$ | 2.1556 | 0.2 | 0.7245 | 0.2256 | −0.2 |
| $BF_{03}^{int}BF_{03}^{ext}$ | 2.1556 | 0.3 | 1.0868 | 0.3384 | −0.3 |
| $BF_{03}^{int}BF_{04}^{ext}$ | 2.1556 | 0.4 | 1.4490 | 0.4512 | −0.4 |
| $BF_{03}^{int}BF_{05}^{ext}$ | 2.1556 | 0.5 | 1.8113 | 0.5640 | −0.5 |
| $BF_{03}^{int}BF_{06}^{ext}$ | 2.1556 | 0.6 | 2.1736 | 0.6768 | −0.6 |
| $BF_{03}^{int}BF_{07}^{ext}$ | 2.1557 | 0.7 | 2.5358 | 0.7897 | −0.7 |
| $BF_{03}^{int}BF_{08}^{ext}$ | 2.1557 | 0.8 | 2.8981 | 0.9025 | −0.8 |

**Table B.4. List of the parameters of the axial velocity profiles for $U_0 = -0.5$, $U_{01} = -0.5$, varying $U_{max}^{ext}$.**

External annular jet

| Test case | $R_{in}^{ext}$ | $U_{max}^{ext}$ | $U_{in}^{ext}$ | $U_{out}^{ext}$ | $U_{01}$ |
|---|---|---|---|---|---|
| $BF_{05}^{int}BF_{05}^{ext}Umax_{04}^{ext}$ | 1.9923 | 0.4 | 2.2074 | 0.4449 | −0.5 |
| $BF_{05}^{int}BF_{05}^{ext}Umax_{06}^{ext}$ | 2.2325 | 0.6 | 1.8082 | 0.6835 | −0.5 |
| $BF_{05}^{int}BF_{05}^{ext}Umax_{07}^{ext}$ | 2.2825 | 0.7 | 1.883 | 0.8038 | −0.5 |

**Table B.5. List of the parameters of the axial velocity profiles for $U_0 = -0.5$.**

Internal annular jet

| Test case | $R_{out}^{int}$ | $U_{in}^{int}$ | $U_{out}^{int}$ | $U_{\infty}$ | $U_0$ |
|---|---|---|---|---|---|
| $BF_{05}^{int}BF_{01}^{ext}$ | 1.1690 | 3.0754 | 2.6935 | −0.58452 | −0.5 |
| $BF_{05}^{int}BF_{02}^{ext}$ | 1.2051 | 2.9598 | 2.6702 | −0.75604 | −0.5 |
| $BF_{05}^{int}BF_{03}^{ext}$ | 1.2387 | 2.8684 | 2.6730 | −0.9333 | −0.5 |
| $BF_{05}^{int}BF_{04}^{ext}$ | 1.2701 | 2.7952 | 2.6959 | −1.1166 | −0.5 |
| $BF_{05}^{int}BF_{05}^{ext}$ | 1.3000 | 2.7334 | 2.7334 | −1.3067 | −0.5 |
| $BF_{05}^{int}BF_{06}^{ext}$ | 1.3283 | 2.6820 | 2.7840 | −1.5036 | −0.5 |
| $BF_{05}^{int}BF_{07}^{ext}$ | 1.3553 | 2.6382 | 2.8454 | −1.7080 | −0.5 |
| $BF_{05}^{int}BF_{08}^{ext}$ | 1.3812 | 2.6004 | 2.9165 | −1.9203 | −0.5 |

External annular jet

| Test case | $R_{in}^{ext}$ | $U_{max}^{ext}$ | $U_{in}^{ext}$ | $U_{out}^{ext}$ | $U_{01}$ |
|---|---|---|---|---|---|
| $BF_{05}^{int}BF_{01}^{ext}$ | 2.1556 | 0.1 | 0.3623 | 0.1128 | −0.1 |
| $BF_{05}^{int}BF_{02}^{ext}$ | 2.1556 | 0.2 | 0.7245 | 0.2256 | −0.2 |
| $BF_{05}^{int}BF_{03}^{ext}$ | 2.1556 | 0.3 | 1.0868 | 0.3384 | −0.3 |
| $BF_{05}^{int}BF_{04}^{ext}$ | 2.1556 | 0.4 | 1.4491 | 0.4512 | −0.4 |
| $BF_{05}^{int}BF_{05}^{ext}$ | 2.1556 | 0.5 | 1.8113 | 0.5640 | −0.5 |
| $BF_{05}^{int}BF_{06}^{ext}$ | 2.1556 | 0.6 | 2.1736 | 0.6768 | −0.6 |
| $BF_{05}^{int}BF_{07}^{ext}$ | 2.1556 | 0.7 | 2.5358 | 0.7897 | −0.7 |
| $BF_{05}^{int}BF_{08}^{ext}$ | 2.1556 | 0.8 | 2.8981 | 0.9025 | −0.8 |

**Table B.6. List of the parameters of the axial velocity profiles for $U_0 = -0.3$, $U_{01} = -0.5$, varying $U^{ext}_{max}$.**

| External annular jet | | | | | |
|---|---|---|---|---|---|
| Test case | $R^{ext}_{in}$ | $U^{ext}_{max}$ | $U^{ext}_{in}$ | $U^{ext}_{out}$ | $U_{01}$ |
| $BF^{int}_{03}BF^{ext}_{05}Umax^{ext}_{04}$ | 1.9924 | 0.4 | 2.2073 | 0.4449 | −0.5 |
| $BF^{int}_{03}BF^{ext}_{05}Umax^{ext}_{06}$ | 2.2325 | 0.6 | 1.8082 | 0.6835 | −0.5 |
| $BF^{int}_{03}BF^{ext}_{05}Umax^{ext}_{07}$ | 2.2826 | 0.7 | 1.8831 | 0.8038 | −0.5 |

## Appendix C. Complex wavenumbers and frequencies of the first absolutely unstable helical mode

**Table C.1. Complex wavenumbers and frequencies for the test cases for $U_0 = 0$.**

| Test case | $\alpha_{0,r}$ | $\alpha_{0,i}$ | $\omega_{0,r}$ | $\omega_{0,i}$ |
|---|---|---|---|---|
| $BF^{int}_{0}BF^{ext}_{01}$ | 1.81463 | −1.43517 | 0.71026 | −0.08734 |
| $BF^{int}_{0}BF^{ext}_{02}$ | 1.75109 | −1.06123 | 0.69334 | 0.05870 |
| $BF^{int}_{0}BF^{ext}_{03}$ | 1.72710 | −0.83300 | 0.65487 | 0.17083 |
| $BF^{int}_{0}BF^{ext}_{04}$ | 1.71304 | −0.65249 | 0.60893 | 0.26359 |
| $BF^{int}_{0}BF^{ext}_{05}$ | 1.70257 | −0.49863 | 0.55939 | 0.34371 |
| $BF^{int}_{0}BF^{ext}_{06}$ | 1.69520 | −0.36200 | 0.50819 | 0.41491 |
| $BF^{int}_{0}BF^{ext}_{07}$ | 1.68844 | −0.24109 | 0.45660 | 0.47963 |
| $BF^{int}_{0}BF^{ext}_{08}$ | 1.68437 | −0.13171 | 0.40560 | 0.53953 |
| $BF^{int}_{0}BF^{ext}_{05}Umax^{ext}_{04}$ | 1.68410 | −0.52077 | 0.54760 | 0.33570 |
| $BF^{int}_{0}BF^{ext}_{05}Umax^{ext}_{06}$ | 1.71859 | −0.47064 | 0.56994 | 0.35415 |
| $BF^{int}_{0}BF^{ext}_{05}Umax^{ext}_{07}$ | 1.73852 | −0.44232 | 0.58135 | 0.36730 |

**Table C.2. Complex wavenumbers and frequencies for the test cases for $U_0 = -0.3$.**

| Test case | $\alpha_{0,r}$ | $\alpha_{0,i}$ | $\omega_{0,r}$ | $\omega_{0,i}$ |
|---|---|---|---|---|
| $BF^{int}_{03}BF^{ext}_{01}$ | 1.58692 | −0.84575 | 0.44884 | 0.10429 |
| $BF^{int}_{03}0BF^{ext}_{02}$ | 1.55857 | −0.85283 | 0.44843 | 0.11973 |
| $BF^{int}_{03}BF^{ext}_{03}$ | 1.55814 | −0.86931 | 0.45904 | 0.14467 |
| $BF^{int}_{03}0BF^{ext}_{04}$ | 1.78256 | −0.77134 | 0.49988 | 0.20427 |
| $BF^{int}_{03}BF^{ext}_{05}$ | 1.74865 | −0.54450 | 0.48371 | 0.30755 |
| $BF^{int}_{03}BF^{ext}_{06}$ | 1.73313 | −0.40186 | 0.44638 | 0.38995 |
| $BF^{int}_{03}BF^{ext}_{07}$ | 1.72477 | −0.27768 | 0.40326 | 0.46161 |
| $BF^{int}_{03}BF^{ext}_{08}$ | 1.71833 | −0.16894 | 0.35800 | 0.52641 |
| $BF^{int}_{03}BF^{ext}_{05}Umax^{ext}_{04}$ | 1.72772 | −0.57714 | 0.470716 | 0.30004 |
| $BF^{int}_{03}BF^{ext}_{05}Umax^{ext}_{06}$ | 1.76676 | −0.50808 | 0.49624 | 0.31874 |
| $BF^{int}_{03}BF^{ext}_{05}Umax^{ext}_{07}$ | 1.79015 | −0.47012 | 0.51059 | 0.33362 |

**Table C.3. Complex wavenumbers and frequencies for the test cases for $U_0 = -0.5$.**

| Test case | $\alpha_{0,r}$ | $\alpha_{0,i}$ | $\omega_{0,r}$ | $\omega_{0,i}$ |
|---|---|---|---|---|
| $BF_{05}^{int}BF_{01}^{ext}$ | 1.460510 | −0.49020 | 0.29383 | 0.20518 |
| $BF_{05}^{int}0BF_{02}^{ext}$ | 1.45278 | −0.50494 | 0.29221 | 0.21275 |
| $BF_{05}^{int}BF_{03}^{ext}$ | 1.44837 | −0.51349 | 0.29433 | 0.22348 |
| $BF_{05}^{int}0BF_{04}^{ext}$ | 1.45331 | −0.53384 | 0.30289 | 0.23889 |
| $BF_{05}^{int}BF_{05}^{ext}$ | 1.49072 | −0.58576 | 0.32468 | 0.26122 |
| $BF_{05}^{int}BF_{06}^{ext}$ | 1.78961 | −0.430295 | 0.37495 | 0.34231 |
| $BF_{05}^{int}BF_{07}^{ext}$ | 1.76301 | −0.27023 | 0.34917 | 0.43509 |
| $BF_{05}^{int}BF_{08}^{ext}$ | 1.75526 | −0.15589 | 0.31275 | 0.50953 |
| $BF_{05}^{int}BF_{05}^{ext}Umax_{04}^{ext}$ | 1.48872 | −0.57005 | 0.31566 | 0.26664 |
| $BF_{05}^{int}BF_{05}^{ext}Umax_{06}^{ext}$ | 1.47900 | −0.60759 | 0.33628 | 0.25416 |
| $BF_{05}^{int}BF_{05}^{ext}Umax_{07}^{ext}$ | 1.44462 | −0.63800 | 0.34955 | 0.24231 |

**Table C.4. Complex wavenumbers and frequencies for the test cases $BF_0^{int}BF_{03}^{ext}$ and $BF_0^{int}BF_{06}^{ext}$ and varying swirl number of the internal jet.**

| | Test case | | | | | | | |
|---|---|---|---|---|---|---|---|---|
| | $BF_0^{int}BF_{03}^{ext}$ | | | | $BF_0^{int}BF_{06}^{ext}$ | | | |
| $A^{int}$ | $\alpha_{0,r}$ | $\alpha_{0,i}$ | $\omega_{0,r}$ | $\omega_{0,i}$ | $\alpha_{0,r}$ | $\alpha_{0,i}$ | $\omega_{0,r}$ | $\omega_{0,i}$ |
| 0.1 | 1.76748 | −0.87990 | 0.66729 | 0.17571 | 1.70551 | −0.37495 | 0.52753 | 0.41904 |
| 0.2 | 1.74977 | −0.95675 | 0.67716 | 0.18302 | 1.70401 | −0.39948 | 0.54689 | 0.41730 |
| 0.3 | 1.66121 | −0.98129 | 0.69809 | 0.19777 | 1.70732 | −0.41139 | 0.56646 | 0.41358 |
| 0.4 | 1.63544 | −0.90354 | 0.73503 | 0.20587 | 1.72044 | −0.41608 | 0.58484 | 0.40747 |
| 0.5 | 1.71823 | −0.83664 | 0.77432 | 0.19391 | 0.17398 | −0.42041 | 0.60148 | 0.39932 |
| 0.6 | 1.82720 | −0.84721 | 0.79939 | 0.17160 | 1.76532 | −0.42091 | 0.61673 | 0.38902 |
| 0.7 | 1.79240 | −0.42372 | 0.63115 | 0.37558 | 1.79240 | −0.42372 | 0.63115 | 0.37558 |
| 0.8 | −− | −− | −− | −− | 1.82016 | −0.42397 | 0.64508 | 0.35710 |
| 0.9 | −− | −− | −− | −− | 1.84480 | −0.42039 | 0.65842 | 0.33035 |

**Table C.5. Complex wavenumbers and frequencies for the test cases $BF_0^{int}BF_{03}^{ext}$ and $BF_0^{int}BF_{06}^{ext}$ and varying swirl number of the external jet.**

| | Test case | | | | | | | |
|---|---|---|---|---|---|---|---|---|
| | $BF_0^{int}BF_{03}^{ext}$ | | | | $BF_0^{int}BF_{06}^{ext}$ | | | |
| $A^{ext}$ | $\alpha_{0,r}$ | $\alpha_{0,i}$ | $\omega_{0,r}$ | $\omega_{0,i}$ | $\alpha_{0,r}$ | $\alpha_{0,i}$ | $\omega_{0,r}$ | $\omega_{0,i}$ |
| 0.1 | 1.78000 | −0.83559 | 0.68787 | 0.15762 | 1.70577 | −0.3723 | 0.53484 | 0.39868 |
| 0.2 | 1.83042 | −0.86060 | 0.71612 | 0.13397 | 1.72188 | −0.38546 | 0.56228 | 0.37870 |
| 0.3 | 1.89535 | −0.90022 | 0.74201 | 0.10775 | 1.73965 | −0.39700 | 0.59069 | 0.35519 |
| 0.4 | 1.98289 | −0.97296 | 0.76118 | 0.08063 | 1.76150 | −0.41238 | 0.62017 | 0.32853 |
| 0.5 | 2.12158 | −1.12779 | 0.76487 | 0.05713 | 0.17398 | −0.42041 | 0.60148 | 0.39932 |
| 0.6 | −− | −− | −− | −− | 1.80684 | −0.44745 | 0.68304 | 0.26872 |
| 0.7 | −− | −− | −− | −− | 1.82205 | −0.47295 | 0.71624 | 0.23822 |
| 0.8 | −− | −− | −− | −− | 1.82500 | −0.52512 | 0.74950 | 0.21060 |

**Table C.6. Complex wavenumbers and frequencies for the test cases $BF_{03}^{int}BF_{03}^{ext}$ and $BF_{03}^{int}BF_{06}^{ext}$ and varying swirl number of the internal jet.**

| | Test case | | | | | | | |
|---|---|---|---|---|---|---|---|---|
| | $BF_{03}^{int}BF_{03}^{ext}$ | | | | $BF_{03}^{int}BF_{06}^{ext}$ | | | |
| $A^{int}$ | $\alpha_{0,r}$ | $\alpha_{0,i}$ | $\omega_{0,r}$ | $\omega_{0,i}$ | $\alpha_{0,r}$ | $\alpha_{0,i}$ | $\omega_{0,r}$ | $\omega_{0,i}$ |
| 0.1 | 1.53346 | −0.78236 | 0.44357 | 0.24524 | 1.73073 | −0.47301 | 0.44183 | 0.40087 |
| 0.2 | 1.51150 | −0.66519 | 0.46394 | 0.32814 | 1.67817 | −0.52097 | 0.44193 | 0.42299 |
| 0.3 | 1.51257 | −0.52926 | 0.50103 | 0.38875 | 1.61652 | −0.48225 | 0.45641 | 0.45010 |
| 0.4 | 1.55209 | −0.39949 | 0.54437 | 0.42562 | 1.61768 | −0.41038 | 0.48339 | 0.46751 |
| 0.5 | 1.60119 | −0.29538 | 0.58753 | 0.43946 | 1.65854 | −0.35149 | 0.51311 | 0.47005 |
| 0.6 | 1.66042 | −0.22207 | 0.62620 | 0.43170 | 1.70786 | −0.31520 | 0.53879 | 0.45835 |
| 0.7 | 1.71488 | −0.17580 | 0.65760 | 0.40367 | 1.74990 | −0.29774 | 0.55660 | 0.43436 |
| 0.8 | 1.760300 | −0.15356 | 0.67959 | 0.35518 | 1.77005 | −0.29526 | 0.56478 | 0.40031 |
| 0.9 | 1.78956 | −0.15406 | 0.68807 | 0.28200 | 1.76042 | −0.29816 | 0.56287 | 0.35804 |

**Table C.7. Complex wavenumbers and frequencies for the test cases $BF_{03}^{int}BF_{03}^{ext}$ and $BF_{03}^{int}BF_{06}^{ext}$ and varying swirl number of the external jet.**

| | Test case | | | | | | | |
|---|---|---|---|---|---|---|---|---|
| | $BF_{03}^{int}BF_{03}^{ext}$ | | | | $BF_{3}^{int}0BF_{06}^{ext}$ | | | |
| $A^{ext}$ | $\alpha_{0,r}$ | $\alpha_{0,i}$ | $\omega_{0,r}$ | $\omega_{0,i}$ | $\alpha_{0,r}$ | $\alpha_{0,i}$ | $\omega_{0,r}$ | $\omega_{0,i}$ |
| 0.1 | 1.55468 | −0.82000 | 0.45516 | 0.17053 | 1.74870 | −0.42748 | 0.46106 | 0.37537 |
| 0.2 | 1.54328 | −0.77258 | 0.45629 | 0.19936 | 1.78290 | −0.44628 | 0.47886 | 0.36154 |
| 0.3 | 1.53795 | −0.72564 | 0.46270 | 0.22681 | 1.80078 | −0.49748 | 0.48733 | 0.34277 |
| 0.4 | 1.51965 | −0.66220 | 0.47383 | 0.25388 | 1.80184 | −0.59147 | 0.48864 | 0.32571 |
| 0.5 | 1.50289 | −0.59530 | 0.48759 | 0.27843 | 1.64511 | −0.63215 | 0.48345 | 0.32294 |
| 0.6 | 1.49066 | −0.52518 | 0.50366 | 0.30058 | 1.58194 | −0.54430 | 0.48978 | 0.33018 |
| 0.7 | 1.47513 | −0.44731 | 0.52169 | 0.32001 | 1.55432 | −0.45931 | 0.50327 | 0.33812 |
| 0.8 | 1.46670 | −0.36131 | 0.54133 | 0.33634 | 1.54232 | −0.36972 | 0.52117 | 0.34531 |
| 0.8 | 1.46253 | −0.26858 | 0.56250 | 0.34930 | 1.54375 | −0.27020 | 0.54206 | 0.35077 |

**Table C.8. Complex wavenumbers and frequencies for the test cases $BF_{05}^{int}BF_{03}^{ext}$ and $BF_{05}^{int}BF_{06}^{ext}$ and varying swirl number of the internal jet.**

| | Test case | | | | | | | |
|---|---|---|---|---|---|---|---|---|
| | $BF_{05}^{int}BF_{03}^{Ixt}$ | | | | $BF_{5}^{int}0BF_{06}^{Ixt}$ | | | |
| $A^{ixt}$ | $\alpha_{0,r}$ | $\alpha_{0,i}$ | $\omega_{0,r}$ | $\omega_{0,i}$ | $\alpha_{0,r}$ | $\alpha_{0,i}$ | $\omega_{0,r}$ | $\omega_{0,i}$ |
| 0.1 | 1.43719 | −0.44869 | 0.29889 | 0.33305 | 1.55140 | −0.51196 | 0.31173 | 0.39045 |
| 0.2 | 1.43877 | −0.35088 | 0.32516 | 0.41730 | 1.50708 | −0.38528 | 0.31093 | 0.45969 |
| 0.3 | 1.46001 | −0.25754 | 0.36229 | 0.47788 | 1.51839 | −0.28802 | 0.33351 | 0.50984 |
| 0.4 | 1.49489 | −0.17096 | 0.40380 | 0.51671 | 1.55081 | −0.21074 | 0.36508 | 0.54133 |
| 0.5 | 1.54086 | −0.09896 | 0.44586 | 0.53576 | 1.59487 | −0.14802 | 0.39880 | 0.55562 |
| 0.6 | 1.58499 | −0.04280 | 0.48597 | 0.53649 | 1.63894 | −0.10457 | 0.43088 | 0.55428 |
| 0.7 | 1.62989 | −0.00190 | 0.52242 | 0.51998 | 1.68206 | −0.07669 | 0.45898 | 0.53869 |
| 0.8 | 1.67165 | 0.02528 | 0.55409 | 0.48665 | 1.71795 | −0.06437 | 0.48182 | 0.50986 |
| 0.9 | 1.70889 | 0.04011 | 0.58021 | 0.43557 | 1.74432 | −0.06684 | 0.49849 | 0.46796 |

**Table C.9. Complex wavenumbers and frequencies for the test cases $BF_{05}^{int}BF_{03}^{ext}$ and $BF_{05}^{int}BF_{06}^{ext}$ and varying swirl number of the external jet.**

| | Test case | | | | | | | |
|---|---|---|---|---|---|---|---|---|
| | $BF_{05}^{int}BF_{03}^{ext}$ | | | | $BF_{05}^{int}BF_{06}^{ext}$ | | | |
| $A^{ext}$ | $\alpha_{0,r}$ | $\alpha_{0,i}$ | $\omega_{0,r}$ | $\omega_{0,i}$ | $\alpha_{0,r}$ | $\alpha_{0,i}$ | $\omega_{0,r}$ | $\omega_{0,i}$ |
| 0.1 | 1.44391 | −0.48403 | 0.29714 | 0.25875 | 1.85765 | −0.56981 | 0.35606 | 0.31899 |
| 0.2 | 1.44206 | −0.44880 | 0.30380 | 0.29049 | 1.53111 | −0.53002 | 0.32451 | 0.34004 |
| 0.3 | 1.43716 | −0.40226 | 0.31346 | 0.31892 | 1.50496 | −0.45616 | 0.31961 | 0.35867 |
| 0.4 | 1.43791 | −0.35142 | 0.32548 | 0.34413 | 1.49121 | −0.39549 | 0.32222 | 0.37524 |
| 0.5 | 1.44102 | −0.29380 | 0.33937 | 0.36612 | 1.48658 | −0.33158 | 0.32980 | 0.38954 |
| 0.6 | 1.44957 | −0.23412 | 0.35474 | 0.38486 | 1.49102 | −0.27190 | 0.34093 | 0.40143 |
| 0.7 | 1.46265 | −0.17542 | 0.37121 | 0.40031 | 1.50451 | −0.20418 | 0.35463 | 0.41073 |
| 0.8 | 1.47923 | −0.11392 | 0.38851 | 0.41244 | 1.52003 | −0.13788 | 0.370147 | 0.41731 |
| 0.9 | 1.50121 | −0.05424 | 0.40635 | 0.42118 | 1.54473 | −0.07505 | 0.38689 | 0.42100 |

## Acknowledgments

This work was supported by the Polish National Science Centre, the grant no. 2016/21/B/ST8/00414.

## References

1. O. Lucca-Negro, T. O'Doherty, *Vortex breakdown: a review*, Progress in Energy and Combustion Science, **27**, 431–481, 2001.
2. N. Syred, *A review of oscillation mechanisms and the role of the precessing vortex core (PVC) in swirl combustion systems*, Progress in Energy and Combustion Science, **32**, 93–161, 2006.
3. K. Oberleithner, C.O. Paschereit, R. Seele, I. Wygnanski, *The formation of turbulent vortex breakdown intermittency, criticality, and global instability*, AIAA Journal, **50**, 7, 1437–1485, 2012.
4. T.B. Benjamin, *Theory of the vortex breakdown phenomenon*, Journal of Fluid Mechanics, **14**, 593–629, 1962.
5. T.B. Benajmin, *Some developments in the theory of vortex breakdown*, Journal of Fluid Mechanics, **28**, 1, 65–84, 1967.
6. H. Bossel, *Vortex breakdown flowfield*, Physics of Fluids, **12**, 3, 498–508, 1969.
7. E. Krause, *A contribution to the problem of vortex breakdown*, Computers and Fluids, **13**, 3, 375–381, 1985.
8. E. Krause, *Numerical prediction of vortex breakdown*, Fluid Dynamics Research, **3**, 3–4, 263–267, 1988.
9. M. Escudier, *Vortex breakdown: observations an explanations*, Progress in Aerospace Science, **25**, 2, 189–229, 1988.
10. L.N. Howard, A.S. Gupta, *On the hydrodynamic and hydromagnetic stability of swirling flows*, Journal of Fluid Mechanics, **14**, 463–76, 1962.

11. M. Lessen, P.J. Singh, F. Paillet, *The stability of a trailing line vortex. Part 1: inviscid theory*, Journal of Fluid Mechanics, **63**, 4, 753–763, 1974.

12. S. Leibovich, K. Stewardson, *A sufficient condition for the instability of columnar vortices*, Journal of Fluid Mechanics, **126**, 335–356, 1983.

13. A.Q. Quadri, D. Mistry, M.P. Juniper, *Structural sensitivity of spiral vortex breakdown*, Journal of Fluid Mechanics, **720**, 558–581, 2013.

14. M. Garcia-Villalba, J. Fröhlich, W. Rodi, *Identification and analysis of coherent structures in the near field of turbulent unconfined annular swirling jets using large eddy simulation*, Physics of Fluids, **18**, 055103, 2006.

15. M. Garcia-Villalba, J. Fröhlich, *LES study of a free annular swirlng jet-Dependence of coherent structures on a pilot jet and the level of swirl*, International Journal of Heat and Fluid Flow, **27**, 911–923, 2006.

16. M. Vaniershot, J.S. Müller, M. Sieber, M. Percin, B.W. van Oudhesden, K. Oberleithner, *Single- and double-helix vortex breakdown as two dominant global modes in turbulent swirling jet flow*, Journal of Fluid Mechanics, **883**, A31, 1–30, 2020.

17. M. Juniper, *Absolute and Convective Instability in Gas Turbine Fuel Injectors*, [in:] ASME Turbo Expo 2012: Turbine Technical Conference and Exposition, **2**, 189–198, 2012.

18. S. Terhaar, K. Oberleithner, C.O. Paschereit, *Key parameters governing the precessing vortex core in reacting flows: an experimental and analytical study*, Proceedings of the Combustion Institute, **35**, 3347–3354, 2015.

19. K. Oberleithner, M. Stöhr, S.H. Im, C.O. Paschereit, *Linear stability analysis of turbulent swirling combustor flows: impact of flow field and flame shapes on the PVC*, [in:] 7th European Combustion Meeting, 2015.

20. A. Michalke, *Absolute inviscid instability of a ring jet with back-flow and swirl*, European Journal of Mechanics-B/Fluids, **18**, 1, 3–12, 1999.

21. R.J. Briggs, *Electron-Stream Interaction with Plasmas*, Research Monograph No. 29, The M.I.T. Press, Cambridge, 1964.

22. A. Bers, *Linear Waves and Instabilities, Physique des Plasmas*, Gordon and Breach, London, 1975.

23. P.J. Schmid, D.S. Henningson, *Stability and Transition in Shear Flows*, Springer, New York, 2001.

24. A. Boguslawski, K. Wawrzak, *Absolute instability of an annular jet: local stability analysis*, Meccanica, An International Journal of Theoretical and Applied Mechanics, **55**, 2179–2198, 2020.

25. K. Wawrzak, A. Boguslawski, A. Tyliszczak, M. Saczek, *LES study of global instability in annular jets*, International Journal of Heat and Fluid Flow, **19**, 18460–12, 2019.

26. T. Broeckhoven, M. Brouns, J. Vanherzeele, S. Vanlanduit, Ch. Lacor, *PIV measurements of double annular jet for validation of numerical simulations*, [in:] 13th International Symposium on Applications of Laser Techniques to Fluid Mechnaics, 2006.

27. T. Frania, S. Geerts, Ch. Hirsch, *Measurements of the 3D turbulent flow field of a confined double annular jet*, [in:] AIAA paper No. 2005-5154, AIAA 4th Theoretical Fluid Mechanics Conference, Toronto, Ontario, 2005.

28. S. GEERTS, CH. HIRSCH, T. BROECKHOVEN, CH. LACOR, *Validation of CFD and turbulence models for confined double annular jets*, [in:] AIAA paper No. 2005-5317, AIAA 4th Theoretical Fluid Mechanics Conference, Toronto, Ontario, 2005.

29. J. BIJAK, A. BOGUSLAWSKI, *Absolute instability of a double ring jet-numerical study*, Journal of Theoretical and Applied Mechanics, **45**, 3, 479–488, 2007.

30. S. JENDOUBI, P. STRYKOWSKI, *Absolute and convective instability of axisymmetric jets with external flow*, Physics of Fluids, **6**, 3000, 1994.

31. A. BOGUSLAWSKI, A. TYLISZCZAK, K. WAWRZAK, *Large eddy simulation predictions of absolutely unstable round hot jet*, Physics of Fluids, **28**, 025108, 2016.

32. E. FEHLBERG, *Low-order classical Runge-Kutta formulas with step size control and their application to some heat transfer problems*, Technical Report 315, NASA, 1969.

33. A. QUARTERONI, R. SACCO, F. SALERI, *Numerical Mathematics*, Springer, New York, 2007.

34. P.A. MONKEWITZ, K.D. SOHN, *Absolute instability in hot jets*, AIAA Journal, **26**, 8, 911–916, 1988.

*Received December 22, 2020; revised version April 15, 2021.*
*Published online June 16, 2021.*